JOURNAL OF PETROLOGY | VOLUME 47 | NUMBER 2 | PAGES 231–254 | 2006 | doi:10.1093/petrology/egi073

# Dissolution of Quartz, Albite, and Orthoclase in $H_2O$-Saturated Haplogranitic Melt at 800°C and 200 MPa: Diffusive Transport Properties of Granitic Melts at Crustal Anatectic Conditions

**ANTONIO ACOSTA-VIGIL*, DAVID LONDON, GEORGE B. MORGAN VI, AND THOMAS A. DEWERS**

SCHOOL OF GEOLOGY AND GEOPHYSICS, UNIVERSITY OF OKLAHOMA, NORMAN, OK 73019, USA

**RECEIVED DECEMBER 26, 2003; ACCEPTED JULY 19, 2005**
**ADVANCE ACCESS PUBLICATION AUGUST 31, 2005**

*We have conducted experiments on dissolution of quartz, albite, orthoclase, and corundum into $H_2O$-saturated haplogranite melt at 800°C and 200 MPa over a duration of 120–1488 h with the aim of ascertaining the diffusive transport properties of granitic melts at crustal anatectic temperatures. Cylinders of anhydrous starting glass and a single mineral phase (quartz or feldspar) were juxtaposed along flat and polished surfaces inside gold or platinum capsules with ≈10 wt % added $H_2O$. Concentration profiles in glass (quenched melt) perpendicular to the mineral–glass interfaces and comparison with relevant phase diagrams suggest that melts at the interface are saturated in the dissolving phases after 384 h, and with longer durations the concentration profiles are controlled only by diffusion of components in the melt. The evolution of the concentration profiles with time indicates that uncoupled diffusion in the melt takes place along the following four linearly independent directions in oxide composition space: $SiO_2$, $Na_2O$, and $K_2O$ axes (Si-, Na-, and K-eigenvectors, respectively), and a direction between the $Al_2O_3$, $Na_2O$, and $K_2O$ axes (Al-eigenvector), such that the Al/Na molar ratio is equal to that of the bulk melt and the Al/(Na + K) molar ratio is equal to the equilibrium ASI (= mol. $Al_2O_3$/[$Na_2O$ + $K_2O$]) of the melt. Experiments in which a glass cylinder was sandwiched between two mineral cylinders—quartz and albite, quartz and K-feldspar, or albite and corundum—tested the validity of the inferred directions of uncoupled diffusion and explored long-range chemical communication in the melt via chemical potential gradients. The application of available solutions to the diffusion equations for the experimental quartz and feldspar dissolution data provides diffusivities along the directions of the Si-eigenvector and Al-eigenvector of ≈(2·0–2·8) × $10^{-15}$ $m^2/s$ and ≈(0·6–2·4) × $10^{-14}$ $m^2/s$, respectively. Minimum diffusivities of alkalis [≈(3–9) × $10^{-11}$ $m^2/s$] are orders of magnitude greater than the tetrahedral components of the melt. The information provided here determines the rate at which crustal anatexis can occur when sufficient heat is supplied and diffusion is the only mass transport (mixing) process in the melt. The calculated diffusivities imply that a quartzo-feldspathic source rock with initial grain size of 2–3 mm undergoing hydrostatic, $H_2O$-saturated melting at 800°C (infinite heat supply) could produce 20–30 vol. % of homogeneous melt in less than 1–10 years. Slower diffusion in $H_2O$-undersaturated melts will increase this time frame.*

KEY WORDS: *chemical diffusion; haplogranite; mineral dissolution experiments; crustal anatexis*

## INTRODUCTION

Mechanical mixing during melt segregation and transport (Wickham, 1987*a*, 1987*b*; Brown *et al.*, 1995) may play a role in homogenizing granitic magmas, but diffusion in the melt ultimately controls the attainment of chemical equilibrium (e.g. Lesher, 1994; Shaw, 2004). Understanding the diffusive transport properties of silicate melts helps to constrain the time frames of some igneous processes that entail the production or

*Corresponding author. Present address: Departamento de Mineralogía y Petrología, Facultad de Ciencias, Universidad de Granada, Fuentenueva s/n, 18002 Granada, Spain. Telephone: +34 958 243358. Fax: +34 958 243368. E-mail: aacosta@ugr.es

homogenization of silicate liquids (e.g. Watson, 1982, 1996; Baker, 1990, 1991; Sawyer, 1991; Lesher, 1994; Barbero *et al.*, 1995; Harris *et al.*, 2000; Acosta-Vigil *et al.*, 2002). Knowledge of the diffusive transport properties of granitic melts can shed light on speciation in the melt that can be tested or augmented by spectroscopic studies [e.g. compare Wolf & London (1994) with Mysen *et al.* (1981, 1999), Gan & Hess (1992) and Toplis & Schaller (1998)]. Accurate information on liquid speciation is essential for constructing rigorous thermodynamic models. The diffusion coefficient matrix (**D**) is a product of the Onsager kinetic matrix (**L**) and a matrix of thermodynamic chemical potentials ($\mu$); thermodynamic properties of the melts can be retrieved through a knowledge of **D** (e.g. Chakraborty, 1995).

This study complements that of Acosta-Vigil *et al.* (2002, 2005) in the investigation of diffusivities and directions of uncoupled chemical diffusion in composition space (e.g. Chakraborty, 1995) in $H_2O$-saturated haplogranitic melts at typical crustal anatectic temperatures. To obtain this information we conducted experiments on dissolution of quartz, albite, orthoclase, and corundum into metaluminous haplogranitic melt at 800°C and 200 MPa $H_2O$. The starting haplogranite melt had the composition of the 200 MPa $H_2O$ minimum (Tuttle & Bowen, 1958), and the ≈115°C interval between eutectic and experimental temperature ensured mineral dissolution and the development of oxide concentration gradients in the melt. Concentration profiles of the oxide components in the glass (quenched melt) were measured perpendicular to the mineral–glass interfaces. Published solutions to the diffusion equations were used, together with constraints provided from the evolution of concentration profiles with time, to determine part of the diffusion matrix of the system by inversion of the concentration profiles. The results confirm the distinctly different behavior of Na and K in relation to Al gradients in the melt (Acosta-Vigil *et al.*, 2002), and can be used to estimate the rate at which melting and melt homogenization can occur during crustal anatexis in an end-member case of infinite (transitory) heat supply and diffusion in the melt as the only mixing mechanism.

## MATERIALS AND METHODS

### Starting materials and experimental methods

The starting materials used in this study include hydrothermal quartz (McCurtain County, Oklahoma, USA), albite (Copelinha, albite I, and Urucum, albite II, both from pegmatite mines in Minas Gerais, Brazil), orthoclase (Little Three pegmatite, California, USA), corundum (source unknown), and synthetic anhydrous metaluminous haplogranite glass (Corning Lab Services, New York, USA) with the nominal composition of the haplogranite eutectic at 200 MPa $H_2O$ (Tuttle & Bowen, 1958). Table 1 shows mean electron microprobe analyses of minerals and starting anhydrous glass and some experimental glasses.

Mineral and glass cylinders ≈1·7 or ≈2·5 mm in diameter and 2–4 mm in length were prepared by drilling the starting materials with diamond coring bits. Mineral and glass cylinder surfaces to be in contact during the experiment were polished flat to a 0·3 μm alumina grit finish. Cores were cleaned with de-ionized, ultra-filtered (DIUF) water in an ultrasonic bath. Mineral and glass cores were loaded inside platinum or gold capsules (≈1·8 or ≈2·6 mm i.d.) with enough DIUF water (≈10 wt %) to ensure saturation of the melt. Capsules were sealed by d.c. argon plasma arc welding while keeping the capsule frozen to prevent volatilization of added water. To ensure no leakage, capsules were placed overnight in an oven at ≈130°C and then reweighed.

Experiments were conducted in water-pressurized NIMONIC 105® cold-seal pressure vessels inclined ≈15° from the horizontal. Capsules were placed with their long axes parallel to the vessels, such that the mineral–melt interfaces remained near vertical during the experiment. Target temperature and pressure were 800°C and 200 MPa, respectively; variations in these target values during the experiments were ≈2°C and 1 MPa. Temperature was monitored with an internal chromel–alumel thermocouple, and pressure was monitored with a factory-calibrated Heise bourdon tube gauge; uncertainties in temperature and pressure are <10°C and <10 MPa, respectively. The samples were first pressurized cold, and then the temperature was raised to the target value at a rate of ≈40°C/min. Oxygen fugacity was controlled indirectly by the composition of the reaction vessels at ≈0·5 log units below the Ni–NiO buffer, based on the $fO_2$ dependence of tin solubility in $H_2O$-saturated haplogranite melts [measured by Wolf *et al.* (1994) and compared with Taylor & Wall (1992) and Linnen *et al.* (1996)]. Experiments were quenched isobarically at a rate of ≈75°C/min using a jet of air and water. After quench, capsules were weighed, punctured, placed in a desiccator overnight, and then reweighed to check for the loss of free water (indicating $H_2O$ saturation at run conditions and providing an estimate of water dissolved into the melt). Products were mounted in Buehler Transoptic® thermal plastic, ground to the center of the cylinders, and polished to a final grit size of 0·3 μm for microprobe analysis.

Two series of experiments were conducted (Table 2): (1) those in which a core of quartz, albite, or orthoclase was juxtaposed against a core of haplogranitic glass (single-mineral dissolution experiments); (2) experiments in which a cylinder of glass was sandwiched between cores of quartz and albite, quartz and orthoclase, or albite

*Table 1: Electron microprobe analyses (wt %) of starting materials and some run products*

| Material: | Starting anhydrous glass | CG 1 glass | Acasi 286 glass | Corundum | Quartz | Albite I | Albite II | Orthoclase |
|---|---|---|---|---|---|---|---|---|
| No. analyses: | 29 | 10 | 88 | 20 | 6 | 20 | 20 | 60 |
| $SiO_2$ | 77·69 (0·51) | 73·58 (0·45) | 72·66 (0·39) | 0·01 (0·01) | 100·68 (0·03) | 68·59 (0·48) | 67·67 (0·35) | 64·96 (0·30) |
| $TiO_2$ | 0·01 (0·01) | 0·01 (0·01) | n.d. | 0·01 (0·01) | 0·00 (0·01) | 0·01 (0·01) | 0·01 (0·02) | n.d. |
| $Al_2O_3$ | 13·02 (0·16) | 11·74 (0·17) | 12·11 (0·16) | 98·50 (0·75) | 0·00 (0·00) | 19·47 (0·18) | 20·00 (0·19) | 18·52 (0·24) |
| FeO* | 0·02 (0·01) | 0·02 (0·01) | n.d. | 0·79 (0·16) | 0·00 (0·00) | 0·01 (0·01) | 0·00 (0·00) | 0·01 (0·01) |
| MnO | 0·00 (0·00) | 0·01 (0·01) | n.d. | 0·00 (0·01) | 0·00 (0·00) | 0·01 (0·01) | 0·01 (0·01) | n.d. |
| MgO | 0·01 (0·00) | 0·01 (0·00) | n.d. | 0·01 (0·00) | 0·00 (0·00) | 0·00 (0·00) | 0·00 (0·00) | n.d. |
| CaO | 0·01 (0·01) | 0·13 (0·10) | 0·02 (0·02) | 0·00 (0·01) | 0·00 (0·00) | 0·06 (0·01) | 0·01 (0·01) | 0·00 (0·00) |
| $Na_2O$ | 4·60 (0·11) | 4·26 (0·12) | 3·95 (0·13) | 0·00 (0·00) | 0·01 (0·01) | 11·61 (0·12) | 11·63 (0·10) | 0·85 (0·06) |
| $K_2O$ | 4·78 (0·09) | 4·64 (0·12) | 4·78 (0·10) | 0·00 (0·00) | 0·00 (0·00) | 0·21 (0·06) | 0·16 (0·04) | 15·35 (0·11) |
| $P_2O_5$ | n.d. | 0·04 (0·02) | n.d. | n.d. | n.d. | n.d. | n.d. | n.d. |
| F | 0·03 | 0·01 (0·02) | n.d. | 0·07 (0·08) | 0·15 (0·10) | 0·04 (0·06) | 0·03 (0·04) | n.d. |
| Cl | 0·01 | 0·01 (0·01) | n.d. | 0·01 (0·00) | 0·00 (0·00) | 0·00 (0·00) | 0·00 (0·00) | n.d. |
| O = F | −0·01 | −0·01 | | −0·03 | −0·06 | −0·02 | −0·01 (0·02) | |
| O = Cl | | | | 0·00 | 0 | 0 | 0·00 (0·00) | |
| Total | 100·17 | 94·45 | | 99·37 | 100·78 | 99·99 | 99·51 | 99·69 |
| $H_2O$ EMPA-diff | | 5·55 | 6·49 | | | | | |
| ASI | 1·020 | 0·956 | 1·035 | | | 1·002 | 1·035 | 1·028 |

*Total Fe expressed as FeO.
n.d., not determined. Numbers in parentheses refer to standard deviations.

and corundum ('sandwiched glass' experiments). The single-mineral dissolution experiments were conducted to obtain concentration gradients of the different oxide components in the liquid resulting from diffusion along different directions in composition space (defined by mineral–glass vectors). The sandwiched glass experiments were conducted to test the validity of the inferred directions of uncoupled diffusion in the melt (see below), to explore the long-range chemical communication in melt via chemical potential gradients (e.g. see the results of the albite–glass–corundum sandwich experiment), and to understand the generation of granite liquids in nature throughout intermediate steps between 'simple' single-mineral dissolution experiments and complex natural rock melting experiments (e.g. Mehnert *et al.*, 1973; Büsch *et al.*, 1974; Arzi, 1978; Acosta-Vigil *et al.*, 2004, and unpublished work in review).

## Analytical methods

Starting materials and experimental products were analyzed with a Cameca SX-50 electron microprobe at the University of Oklahoma. Matrix reduction used the PAP correction algorithm (Pouchou & Pichoir, 1985). Mineral phases were analyzed using an accelerating voltage of 20 kV, a beam current of 10 nA, and a 3 μm spot size. Counting times for all elements except Ca, Ba, Sr and Fe were 30 s on peak, 45 s for Ca, Ba and Sr, and 60 s for Fe. Calculated 3σ minimum detection limits (in wt %) were 0·06 for $SiO_2$, 0·03 for $Al_2O_3$ and $Na_2O$, 0·01 for CaO and $K_2O$, 0·02 for $Fe_2O_3$, 0·05 for $P_2O_5$, 0·09 for BaO, and 0·07 for SrO. The glasses were analyzed using an accelerating voltage of 20 kV, a beam current of 2 nA, and a 20 μm defocused spot. Sodium, potassium, and aluminum were concurrently analyzed first to minimize alkali volatilization and attendant changes in elemental ratios. Counting times were 30 s on peak for all elements, yielding calculated 3σ minimum detection limits of $\leq$0·02 wt % for $Na_2O$, $K_2O$ and $Al_2O_3$, and $\approx$0·05 wt % for $SiO_2$. Based on counting statistics, analytical uncertainties relative to their reported concentrations in glass are in the range of $\approx$0·5–1·0 % for $SiO_2$ and $Al_2O_3$, and $\approx$1·5–3·0 % for $Na_2O$ and $K_2O$. Using these methods, the loss of sodium and grow-in of aluminum and silicon intensities during analysis are negligible and comparable with or less than the analytical uncertainties, so that no corrections to the data are needed (Morgan & London, 1996). $H_2O$ concentrations in glass are calculated by difference of the electron microprobe analyses totals from 100%. The accuracy of water by difference, using the current analytical methods, is equal to or better than ±10% relative (Morgan & London, 1996; Acosta-Vigil *et al.*, 2003). The maximum uncertainty for the reported ASI values is ±0·035 (ASI = mol. $Al_2O_3$/[CaO + $Na_2O$ + $K_2O$]), calculated by the propagation of errors. To ensure (1) that diffusion in the melt occurred

*Table 2: Starting materials, duration, and some features of the conducted experiments*

| Run no. | Starting materials | $H_2O$* (wt %) | Duration (h) | Interface retreat (μm) | Width boundary layer (μm) |
|---|---|---|---|---|---|
| CG 1 | $H_2O$ + Dry haplogranite glass rod | 7·50 | 240 | | |
| Acasi 228 | $H_2O$ + Dry haplogranite glass rod + Quartz rod | 10·99 | 120 | 0·5 | 20 |
| Acasi 146-1 | $H_2O$ + Dry haplogranite glass rod + Quartz rod | 14·21 | 240 | 0·9 | 60 |
| Acasi 227 | $H_2O$ + Dry haplogranite glass rod + Quartz rod | 10·45 | 384 | 1·3 | 110 |
| Acasi 220 | $H_2O$ + Dry haplogranite glass rod + Quartz rod | 12·30 | 768 | 2·0 | 200 |
| Acasi 239 | $H_2O$ + Dry haplogranite glass rod + Quartz rod | 10·35 | 1008 | 2·2 | 230 |
| Acasi 236 | $H_2O$ + Dry haplogranite glass rod + Quartz rod | 9·68 | 1488 | 3·7 | 290 |
| Acasi 230 | $H_2O$ + Dry haplogranite glass rod + Albite II rod | 10·39 | 120 | 3·0 | 50 |
| Acasi 147-1 | $H_2O$ + Dry haplogranite glass rod + Albite I rod | 11·60 | 240 | 14·0 | 150 |
| Acasi 229 | $H_2O$ + Dry haplogranite glass rod + Albite II rod | 10·87 | 384 | 41·6 | 340 |
| Acasi 152 | $H_2O$ + Dry haplogranite glass rod + Albite I rod | 10·90 | 960 | 49·0 | 450 |
| Acasi 286 | $H_2O$ + Dry haplogranite glass rod + Orthoclase rod | 10·15 | 69 | | <50 |
| Acasi 231 | $H_2O$ + Dry haplogranite glass rod + Orthoclase rod | 10·42 | 120 | 6·4 | 80 |
| Acasi 145-1 | $H_2O$ + Dry haplogranite glass rod + Orthoclase rod | 14·36 | 240 | 12·5 | 120 |
| Acasi 292 | $H_2O$ + Pre-hydrated haplogranite glass rod + Orthoclase rod | 1·18 | 384 | | 240 |
| Acasi 232 | $H_2O$ + Dry haplogranite glass rod + Orthoclase rod | 11·17 | 384 | 21·6 | 230 |
| Acasi 238 | $H_2O$ + Dry haplogranite glass rod + Orthoclase rod | 10·55 | 768 | 20·4 | 260 |
| Acasi 150 | $H_2O$ + Dry haplogranite glass rod + Orthoclase rod | 11·28 | 960 | 38·1 | 420 |
| Acasi 235 | $H_2O$ + Dry haplogranite glass rod + Orthoclase rod | 10·29 | 1488 | 30·8 | 440 |
| Acasi 261 | $H_2O$ + Quartz rod + Dry haplogranite glass rod + Albite rod | 11·31 | 792 | | |
| Acasi 262 | $H_2O$ + Quartz rod + Dry haplogranite glass rod + Orthoclase rod | 11·17 | 792 | | |
| Acasi 263 | $H_2O$ + Corundum rod + Dry haplogranite glass rod + Albite rod | 10·47 | 720 | | |

All the experiments were run at 800°C and 200 MPa $H_2O$.
*Proportion of water sealed inside the capsule with respect to the haplogranite glass.

only in the direction perpendicular to the mineral–melt interface, and (2) statistical accuracy at critical points in the diffusion profile, we conducted several analytical transverses throughout the experimental glasses: three transverses perpendicular to the mineral–melt interface for each experiment—one at the center of the cylinder and two more at ≈100–200 μm from each of the cylinder sides—plus two additional transverses parallel to the interface at distances of ≈30 and ≈100 μm from the interface.

## RESULTS

### Run products and dissolution rates

The experiments involved dissolution of the starting mineral phase(s) into the melt, with no significant new mineral growth in the silicate liquid or at the mineral–melt interface. Mineral–melt interfaces for quartz and corundum remained flat during dissolution, but these became irregular at the 10–100 μm scale during feldspar dissolution (Fig. 1). Back-scattered electron imaging shows no recrystallization or alteration of quartz, orthoclase, or corundum during the experiments. Albite, however, shows minor recrystallization to a binary feldspar solid solution, mostly along fractures connected to the interface (Fig. 1, Table 3). With this exception, relict feldspars close to the interface melt show no change in composition with respect to the starting feldspars (Table 3).

Dissolution rates were calculated by mass balance using starting and final $SiO_2$ and $Al_2O_3$ concentration profiles in the glass, together with quartz, albite, and orthoclase compositions. This method indicates a retreat of the interfaces proportional to the square root of time after ≈120–384 h (Fig. 2), suggesting that dissolution is interface reaction-controlled up to 120–384 h and becomes diffusion-controlled afterwards (e.g. Cooper & Kingery, 1964).

### Chemical composition of the glasses

All experimental glass columns are characterized by (1) a reaction–diffusion zone adjacent to the mineral–glass interfaces, hereafter referred as the 'boundary layer', in which gradients in the concentration profiles of the

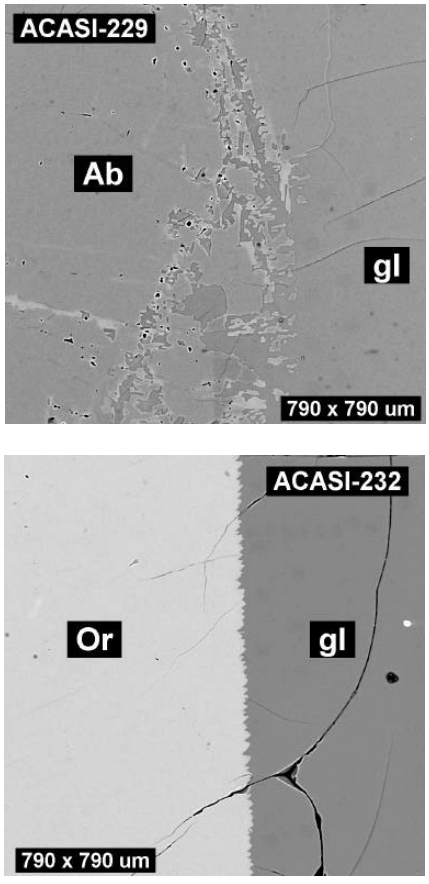


**Fig. 1.** Back-scattered electron images of mineral–glass interfaces in experiments Acasi 229 (albite dissolution) and Acasi 232 (orthoclase dissolution). Light gray domains in Acasi 229 correspond to a binary feldspar recrystallized after the starting albite. Mineral symbols are taken from Kretz (1983); gl, glass.

oxide components are present, and (2) a zone beyond the boundary layer in which the concentration profiles are flat.

*Single-mineral dissolution experiments*

After 384 h, the compositions of glasses within the boundary layer at ≈20 μm from mineral–melt interfaces lie very close to the liquidus surfaces for the respective minerals in the $H_2O$-saturated quartz–albite–orthoclase system at the experimental conditions (≈5–10 normative wt % off the 800°C liquidus isotherms as taken from Tuttle & Bowen, 1958) (Fig. 3). Feldspars and interface melts are not strictly in equilibrium because the feldspars should be binary and not end-members (see Tuttle & Bowen, 1958). Albite shows signs of very local equilibration with the interface melt in the timeframe of the experiments; orthoclase does not. The location of the interface melts very close to the liquidus surfaces after 384 h of run duration, however, strongly suggests that they are saturated in the dissolving mineral phases.

The dissolution of quartz vs feldspars produced contrasting concentration profiles in the melt. Quartz dissolution involved mainly addition of silica and dilution of alumina and alkalis in the boundary layer. Beyond the boundary layer, the concentrations of silica, alumina, and alkalis are similar to those in the starting hydrated glass (Table 4, Fig. 4). The molar ratios Al/Na, Al/K, and Na/K remained nearly constant throughout the entire melt column and equal to the values in the starting hydrous glass (Fig. 4, see insets). These facts indicate that diffusion of silicon occurs only within the boundary layer and does not involve coupling with any other component in melt.

Upon dissolution of albite, the concentrations of alumina, sodium, and potassium in the glass increase monotonically within the boundary layer toward the mineral–glass interface, whereas silica decreases (Table 4, Fig. 5). Beyond the boundary layer, the concentrations of alumina and silica and the Al/Si molar ratios are similar to those in the starting hydrated glass, whereas alkali concentrations and Na/Si and K/Si molar ratios change significantly with respect to the starting glass (Table 4). This indicates that diffusion of aluminum and silicon takes place only within the boundary layer, whereas alkalis diffuse throughout the entire (≈2000–4000 μm long) melt column. This further reveals (1) that alkalis can diffuse much faster than silicon and aluminum, and (2) that aluminum and sodium decouple upon entering the melt during the dissolution of albite. By 'decouple' we mean that although a certain amount of sodium or potassium diffuses together with aluminum (the concentration profiles of alkalis match exactly those of alumina in all the runs), the rest diffuses further beyond the boundary layer and therefore diffuses independently of aluminum. Although the shapes of the concentration profiles for both alkalis are similar in albite dissolution runs, the direction of diffusion for sodium is opposite to that for diffusion of potassium: sodium diffuses downhill away from the interface, producing an increase in its concentration throughout the melt column with respect to the starting glass, and potassium diffuses uphill toward the interface, with an overall decrease in its concentration (Fig. 5). These changes in concentration are above analytical uncertainties.

Orthoclase dissolution experiments yield observations comparable with those for albite (Fig. 6). The migration of aluminum and silicon takes place only within the boundary layer, whereas alkalis diffuse throughout the entire melt reservoir. Upon entering the melt, aluminum and potassium (from orthoclase) become decoupled. Potassium diffuses down its concentration gradient away from the interface, increasing its concentration throughout the melt, whereas sodium diffuses uphill toward the interface, decreasing its concentration in the melt beyond the boundary layer.

*Table 3: Electron microprobe analyses (wt %) of feldspars after the experiments*

| Run no.: | Acasi 147-1 | Acasi 147-1 | Acasi 229 | Acasi 229 | Acasi 232 | Acasi 150 |
|---|---|---|---|---|---|---|
| Material: | Relict albite I* | Recrystallized feldspar | Relict albite II* | Recrystallized feldspar | Relict orthoclase† | Relict orthoclase† |
| No. analyses: | 7 | 6 | 6 | 5 | 10 | 10 |
| $SiO_2$ | 68·60 (0·12) | 67·37 (0·37) | 68·58 (0·12) | 67·29 (0·40) | 64·85 (0·11) | 64·81 (0·31) |
| $Al_2O_3$ | 19·43 (0·09) | 19·43 (0·27) | 19·66 (0·07) | 19·79 (0·12) | 18·36 (0·07) | 18·54 (0·10) |
| CaO | 0·06 (0·01) | 0·13 (0·05) | 0·08 (0·01) | 0·26 (0·13) | 0·00 (0·01) | 0·01 (0·01) |
| $Na_2O$ | 11·53 (0·12) | 7·91 (0·45) | 11·50 (0·08) | 9·91 (0·40) | 0·93 (0·03) | 1·01 (0·04) |
| $K_2O$ | 0·17 (0·03) | 5·24 (0·67) | 0·28 (0·00) | 2·50 (0·64) | 15·35 (0·05) | 15·37 (0·07) |
| Total | 99·79 (0·19) | 100·08 (0·46) | 100·10 (0·14) | 99·75 (0·12) | 99·49 (0·13) | 99·74 (0·43) |

*Albite composition at 10 μm from the interface.
†Average of two five-analysis transverses perpendicular to the interface (30 μm spacing, first point at 20 μm from interface).
Numbers in parenthesis refer to standard deviations.

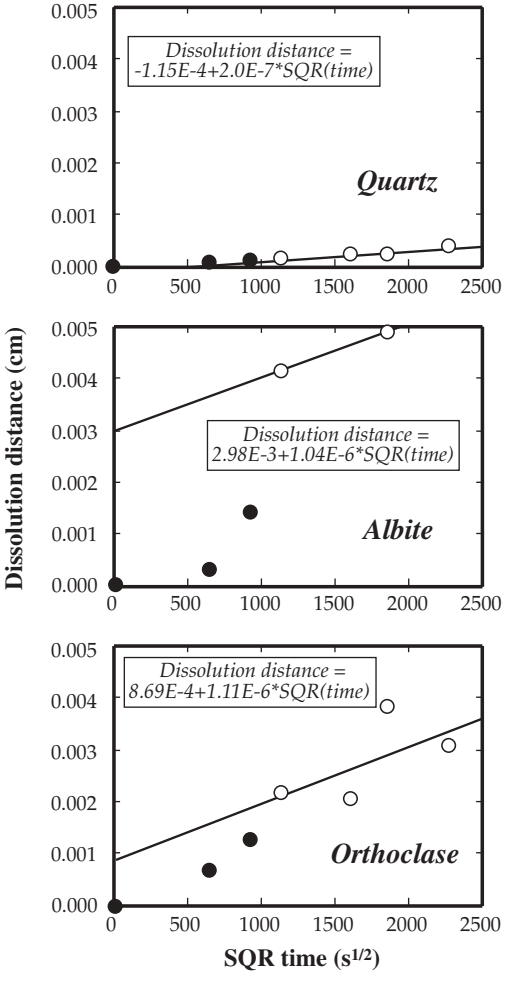


**Fig. 2.** Retreat of the quartz–, albite–, and orthoclase–melt interfaces (dissolution distance) vs the square root of time, calculated by mass balance based on starting and final silica and alumina concentration profiles in the glasses.

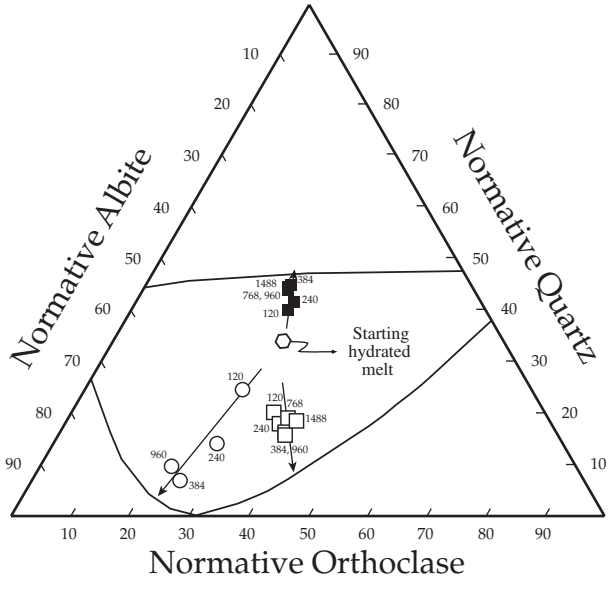


**Fig. 3.** Normative composition (wt %) of starting hydrated melt and experimental glasses at 25 μm from the mineral–glass interfaces in the quartz (■), albite (○), and orthoclase (□) dissolution experiments. Each point represents the mean value of three analyses along the interface. Numbers close to the points refer to run duration in hours. The curved lines correspond to the projections of the liquidus surfaces of quartz and feldspar in the haplogranite system at the experimental conditions (from Tuttle & Bowen, 1958).

We note that in all the feldspar dissolution experiments, the Al/Na molar ratio is constant at any time throughout the entire melt (Table 4, Figs 5 and 6). As the Al/Na ratio in the starting glass (≈1·75) is different from that in albite (≈1) and orthoclase (≫1·75), and diffusion of aluminum occurs only within the boundary layer, these observations require that sodium diffuses throughout the entire melt column to erase any gradient in the Al/Na molar ratio.

*Table 4: Oxide concentrations (in wt %) and molar ratios in the glasses of the single mineral dissolution and sandwiched glass experiments, along analytical transverses perpendicular to the mineral–glass interfaces*

| Run no. | Duration (h) | $SiO_2$ | $Al_2O_3$ | $Na_2O$ | $K_2O$ | $H_2O$[a] | ASI | Al/Si[b] | Al/Na[b] | Al/K[b] | Na/K[b] | $SiO_2$ | $Al_2O_3$ | $Na_2O$ | $K_2O$ | $H_2O$[a] | ASI | Al/Si[b] | Al/Na[b] | Al/K[b] | Na/K[b] | $SiO_2$ | $Al_2O_3$ | $Na_2O$ | $K_2O$ | $H_2O$[a] | ASI | Al/Si[b] | Al/Na[b] | Al/K[b] | Na/K[b] |
|---|---|---|---|---|---|---|---|---|---|---|---|---|---|---|---|---|---|---|---|---|---|---|---|---|---|---|---|---|---|---|---|
| | | *Glass composition at 20 μm from the interface* | | | | | | | | | | *Glass composition at 200 μm from the interface* | | | | | | | | | | *Glass composition beyond the boundary layer* | | | | | | | | | |
| **Quartz dissolution experiments** | | | | | | | | | | | | | | | | | | | | | | | | | | | | | | | |
| Acasi 228 | 120 | 75·15 | 11·02 | 3·65 | 4·25 | 5·93 | 1·040 | 0·173 | 1·84 | 2·40 | 1·31 | 73·67 | 11·80 | 4·07 | 4·44 | 6·01 | 1·025 | 0·189 | 1·76 | 2·46 | 1·39 | 73·58 | 11·86 | 4·14 | 4·47 | 5·93 | 1·016 | 0·190 | 1·74 | 2·45 | 1·41 |
| Acasi 146-1 | 240 | 74·06 | 10·78 | 3·37 | 4·18 | 7·59 | 1·066 | 0·171 | 1·94 | 2·38 | 1·22 | 71·91 | 11·94 | 3·95 | 4·48 | 7·71 | 1·050 | 0·196 | 1·84 | 2·46 | 1·34 | 72·31 | 11·98 | 3·98 | 4·45 | 7·26 | 1·052 | 0·195 | 1·83 | 2·49 | 1·36 |
| Acasi 227 | 384 | 75·87 | 10·38 | 3·31 | 3·92 | 6·50 | 1·069 | 0·161 | 1·91 | 2·44 | 1·28 | 73·18 | 11·87 | 4·00 | 4·41 | 6·52 | 1·044 | 0·191 | 1·80 | 2·49 | 1·38 | 72·98 | 11·94 | 4·09 | 4·42 | 6·56 | 1·035 | 0·193 | 1·78 | 2·49 | 1·40 |
| Acasi 220 | 768 | 75·93 | 10·34 | 3·43 | 3·89 | 6·41 | 1·050 | 0·161 | 1·83 | 2·46 | 1·34 | 73·79 | 11·56 | 4·18 | 4·37 | 6·06 | 0·990 | 0·185 | 1·68 | 2·45 | 1·45 | 73·13 | 11·90 | 4·13 | 4·46 | 6·38 | 1·021 | 0·192 | 1·75 | 2·46 | 1·41 |
| Acasi 239 | 1008 | 76·23 | 10·01 | 3·44 | 3·95 | 6·37 | 1·006 | 0·155 | 1·77 | 2·34 | 1·33 | 73·70 | 11·42 | 3·92 | 4·31 | 6·63 | 1·025 | 0·183 | 1·77 | 2·45 | 1·38 | 73·30 | 11·98 | 4·08 | 4·44 | 6·18 | 1·038 | 0·193 | 1·79 | 2·49 | 1·39 |
| Acasi 236 | 1488 | 76·77 | 9·91 | 3·48 | 3·93 | 5·88 | 0·987 | 0·152 | 1·73 | 2·33 | 1·35 | 74·01 | 11·47 | 4·03 | 4·43 | 6·05 | 1·003 | 0·183 | 1·73 | 2·39 | 1·38 | 73·13 | 11·89 | 4·17 | 4·49 | 6·30 | 1·012 | 0·192 | 1·73 | 2·45 | 1·41 |
| **Albite dissolution experiments** | | | | | | | | | | | | | | | | | | | | | | | | | | | | | | | |
| Acasi 230 | 120 | 70·24 | 13·64 | 5·35 | 4·28 | 6·47 | 1·013 | 0·229 | 1·55 | 2·94 | 1·90 | 73·55 | 11·60 | 4·37 | 4·11 | 6·35 | 0·993 | 0·186 | 1·61 | 2·61 | 1·62 | 73·52 | 11·72 | 4·48 | 4·00 | 6·27 | 0·999 | 0·188 | 1·59 | 2·71 | 1·70 |
| Acasi 147-1 | 240 | 66·30 | 15·80 | 6·32 | 4·30 | 7·22 | 1·043 | 0·281 | 1·52 | 3·39 | 2·23 | 73·04 | 11·99 | 4·77 | 3·89 | 6·29 | 0·992 | 0·193 | 1·53 | 2·85 | 1·86 | 73·07 | 11·87 | 4·58 | 3·86 | 6·60 | 1·010 | 0·191 | 1·57 | 2·84 | 1·81 |
| Acasi 229 | 384 | 64·05 | 17·27 | 7·38 | 3·91 | 7·34 | 1·048 | 0·318 | 1·42 | 4·08 | 2·87 | 68·12 | 14·84 | 6·30 | 3·72 | 7·00 | 1·030 | 0·257 | 1·43 | 3·68 | 2·57 | 73·33 | 11·83 | 4·91 | 3·27 | 6·65 | 1·017 | 0·190 | 1·47 | 3·34 | 2·28 |
| Acasi 152 | 960 | 65·54 | 16·70 | 7·39 | 3·52 | 6·82 | 1·042 | 0·300 | 1·37 | 4·39 | 3·19 | 68·33 | 15·31 | 6·59 | 3·55 | 6·21 | 1·042 | 0·264 | 1·41 | 3·99 | 2·82 | 73·83 | 12·00 | 5·10 | 3·11 | 5·95 | 1·019 | 0·192 | 1·43 | 3·57 | 2·49 |
| **Orthoclase dissolution experiments** | | | | | | | | | | | | | | | | | | | | | | | | | | | | | | | |
| Acasi 231 | 120 | 68·15 | 14·58 | 4·97 | 5·36 | 6·93 | 1·040 | 0·252 | 1·78 | 2·51 | 1·41 | 72·94 | 11·94 | 3·79 | 4·95 | 6·37 | 1·027 | 0·193 | 1·91 | 2·23 | 1·16 | 72·70 | 11·69 | 3·86 | 4·84 | 6·88 | 1·007 | 0·190 | 1·84 | 2·23 | 1·21 |
| Acasi 145-1 | 240 | 67·09 | 14·78 | 4·98 | 5·64 | 7·47 | 1·030 | 0·260 | 1·80 | 2·42 | 1·34 | 72·34 | 12·05 | 3·78 | 4·91 | 6·90 | 1·042 | 0·197 | 1·94 | 2·27 | 1·17 | 72·12 | 11·76 | 3·79 | 4·90 | 7·40 | 1·018 | 0·192 | 1·89 | 2·22 | 1·18 |
| Acasi 232 | 384 | 66·23 | 15·47 | 4·93 | 5·96 | 7·37 | 1·057 | 0·275 | 1·91 | 2·40 | 1·26 | 70·93 | 12·75 | 3·97 | 5·34 | 6·97 | 1·030 | 0·212 | 1·95 | 2·21 | 1·13 | 72·93 | 11·84 | 3·69 | 5·09 | 6·44 | 1·021 | 0·191 | 1·95 | 2·15 | 1·10 |
| Acasi 238 | 768 | 67·69 | 15·08 | 4·77 | 5·88 | 6·56 | 1·057 | 0·262 | 1·92 | 2·37 | 1·23 | 70·96 | 12·80 | 3·90 | 5·63 | 6·69 | 1·019 | 0·213 | 1·99 | 2·10 | 1·05 | 72·80 | 11·98 | 3·55 | 5·32 | 6·34 | 1·031 | 0·194 | 2·05 | 2·08 | 1·01 |
| Acasi 150 | 960 | 66·80 | 15·56 | 5·00 | 6·00 | 6·56 | 1·047 | 0·275 | 1·89 | 2·40 | 1·27 | 69·28 | 14·11 | 4·46 | 5·77 | 6·36 | 1·036 | 0·240 | 1·92 | 2·26 | 1·17 | 73·25 | 11·92 | 3·57 | 5·24 | 6·00 | 1·030 | 0·192 | 2·03 | 2·10 | 1·04 |
| Acasi 235 | 1488 | 67·47 | 15·11 | 4·61 | 6·11 | 6·66 | 1·060 | 0·264 | 1·99 | 2·28 | 1·15 | 70·19 | 13·64 | 4·05 | 5·77 | 6·35 | 1·056 | 0·229 | 2·05 | 2·18 | 1·07 | 72·83 | 12·01 | 3·45 | 5·34 | 6·33 | 1·046 | 0·195 | 2·11 | 2·08 | 0·98 |
| | | *Glass at 25 μm from left interface*[c] | | | | | | | | | | *Glass between boundary layers* | | | | | | | | | | *Glass at 25 μm from right interface*[d] | | | | | | | | | |
| **Sandwiched glass experiments** | | | | | | | | | | | | | | | | | | | | | | | | | | | | | | | |
| Acasi 261 | 792 | 76·53 | 10·26 | 4·15 | 3·05 | 6·01 | 1·013 | 0·158 | 1·50 | 3·11 | 2·07 | 73·46 | 11·80 | 4·92 | 3·35 | 6·48 | 1·003 | 0·189 | 1·46 | 3·25 | 2·23 | 65·68 | 15·94 | 6·80 | 3·93 | 7·60 | 1·029 | 0·286 | 1·43 | 3·75 | 2·63 |
| Acasi 262 | 792 | 76·43 | 10·04 | 2·84 | 4·70 | 5·99 | 1·028 | 0·155 | 2·15 | 1·97 | 0·92 | 72·65 | 11·80 | 3·49 | 5·31 | 6·74 | 1·027 | 0·192 | 2·06 | 2·06 | 1·00 | 67·27 | 14·79 | 4·59 | 6·04 | 7·29 | 1·047 | 0·259 | 1·96 | 2·26 | 1·15 |
| Acasi 263 | 720 | 66·14 | 16·48 | 6·43 | 4·08 | 6·83 | 1·093 | 0·294 | 1·56 | 3·74 | 2·40 | 73·70 | 12·21 | 4·71 | 3·62 | 5·81 | 1·045 | 0·197 | 1·57 | 3·13 | 1·98 | 65·75 | 16·82 | 6·45 | 4·12 | 6·85 | 1·116 | 0·302 | 1·59 | 3·77 | 2·38 |

[a]Calculated by the electron microprobe analyses difference method.
[b]Molar ratio.
[c]Left interface corresponds to quartz–glass in Acasi 261 and Acasi 262, and corundum–glass in Acasi 263 (see Fig. 7).
[d]Right interface corresponds to albite–glass in Acasi 261 and Acasi 263, and orthoclase–glass in Acasi 262 (see Fig. 7).

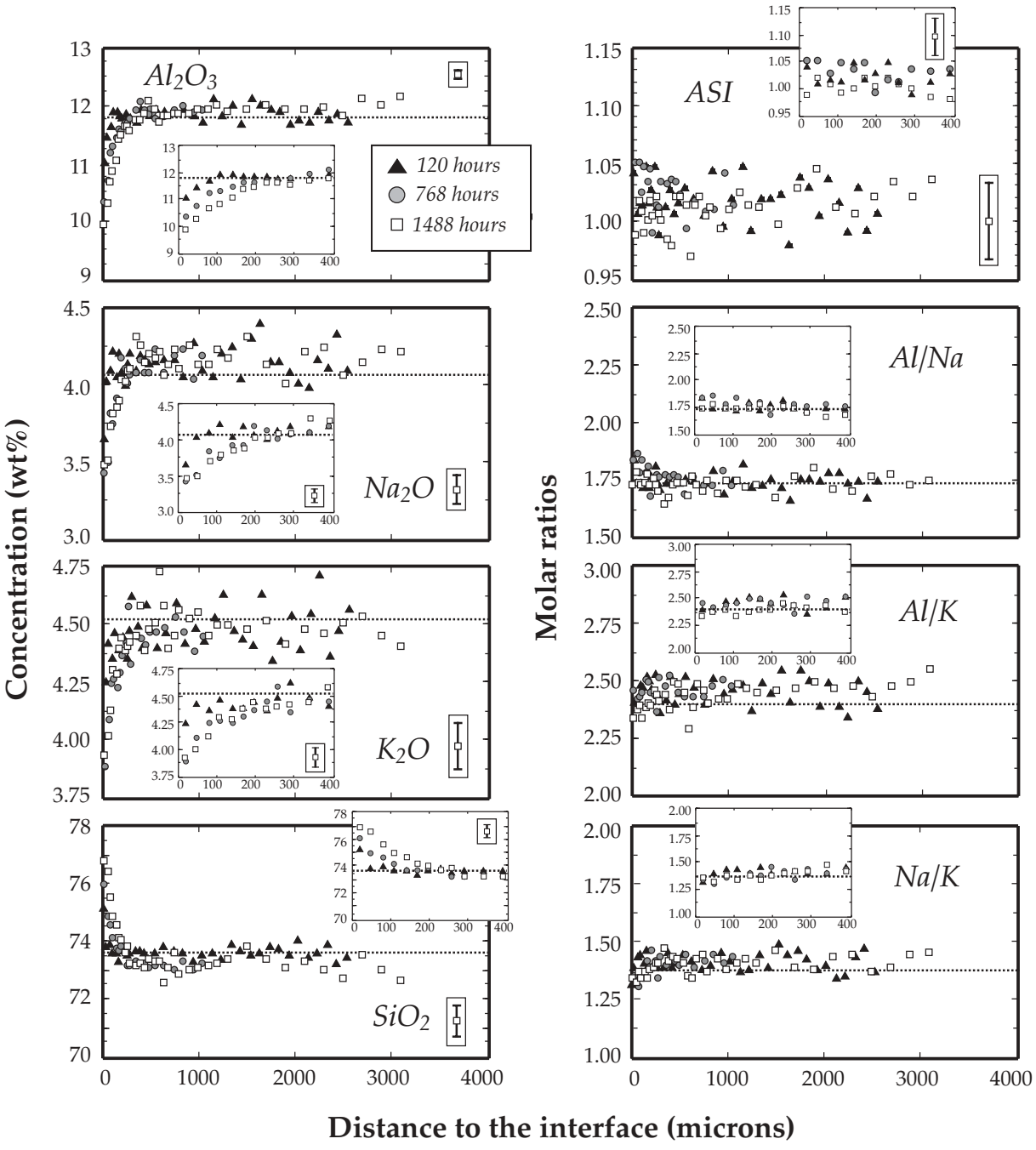


**Fig. 4.** Composition of glasses in the quartz dissolution experiments as a function of experimental time and distance to the quartz–glass interface. In this and subsequent figures, each concentration profile represents the mean values of three analytical transverses perpendicular to the interface; the compositions are shown as obtained from the electron microprobe; the dashed lines refer to concentrations or molar ratios in the starting $H_2O$-saturated metaluminous melt; analytical uncertainties (error bars) are shown within rectangles (analytical uncertainties are equal to or smaller than the symbols when not shown).

Despite the large fluxes of alkalis in opposite directions, the ASI throughout the entire melt column at any experimental time remains constant within analytical uncertainty, and equal to the ASI of melt at equilibrium, ASI $\approx 1{\cdot}025 \pm 0{\cdot}035$.

### *Sandwiched glass experiments*

*Metaluminous haplogranite system*. The experiments in which glass was sandwiched between quartz and feldspars produced results comparable with those of the single-mineral dissolution experiments (Table 4, Fig. 7). Silica

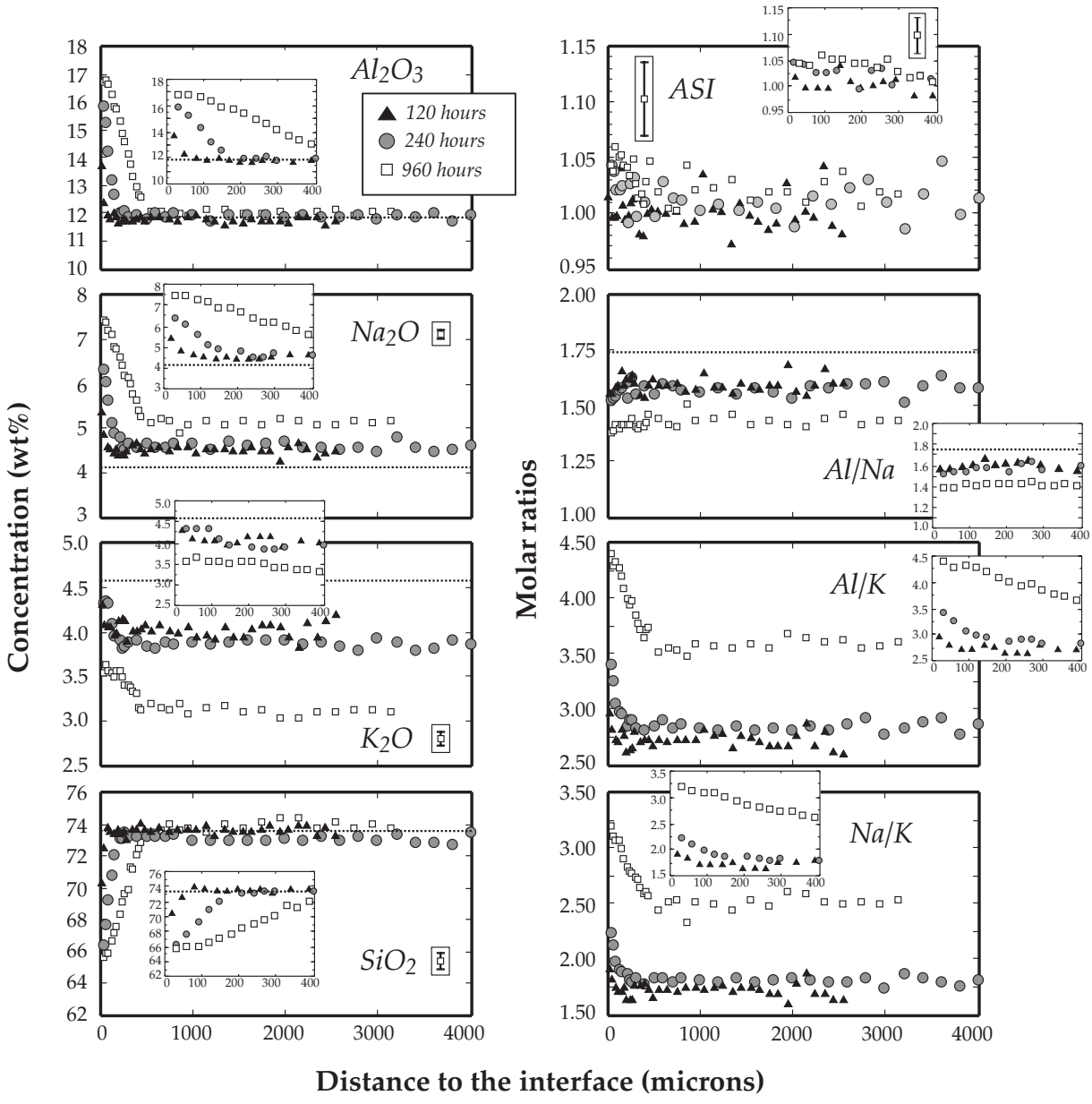


**Fig. 5.** Composition of glasses in the albite dissolution experiments as a function of experimental time and distance to the albite–glass interface.

concentration in the glass increases toward quartz and decreases toward feldspars. Alumina and alkali concentrations increase toward feldspars and decrease toward quartz. The Al/Na molar ratio is constant throughout the glass. The Al/K molar ratio is constant except within the boundary layer close to feldspars, where it increases toward the interface. The ASI is constant throughout the glass except in the boundary layers close to feldspars, where it increases slightly toward the interfaces, although it remains constant within analytical uncertainty.

*Peraluminous haplogranite system*. The only significant differences between the sandwich experiment in the peraluminous system (corundum–glass–albite) and those in the metaluminous system are the greater ASI values throughout the entire glass and the notable increase in ASI within the boundary layers toward corundum and, importantly, toward albite as well (Table 4, Fig. 7).

## Effects of glass hydration–melting and an $H_2O$ fluid phase

The starting glass cores are anhydrous. For the correct interpretation of results, it is important to determine if hydration–melting of the glass cores is complete prior to

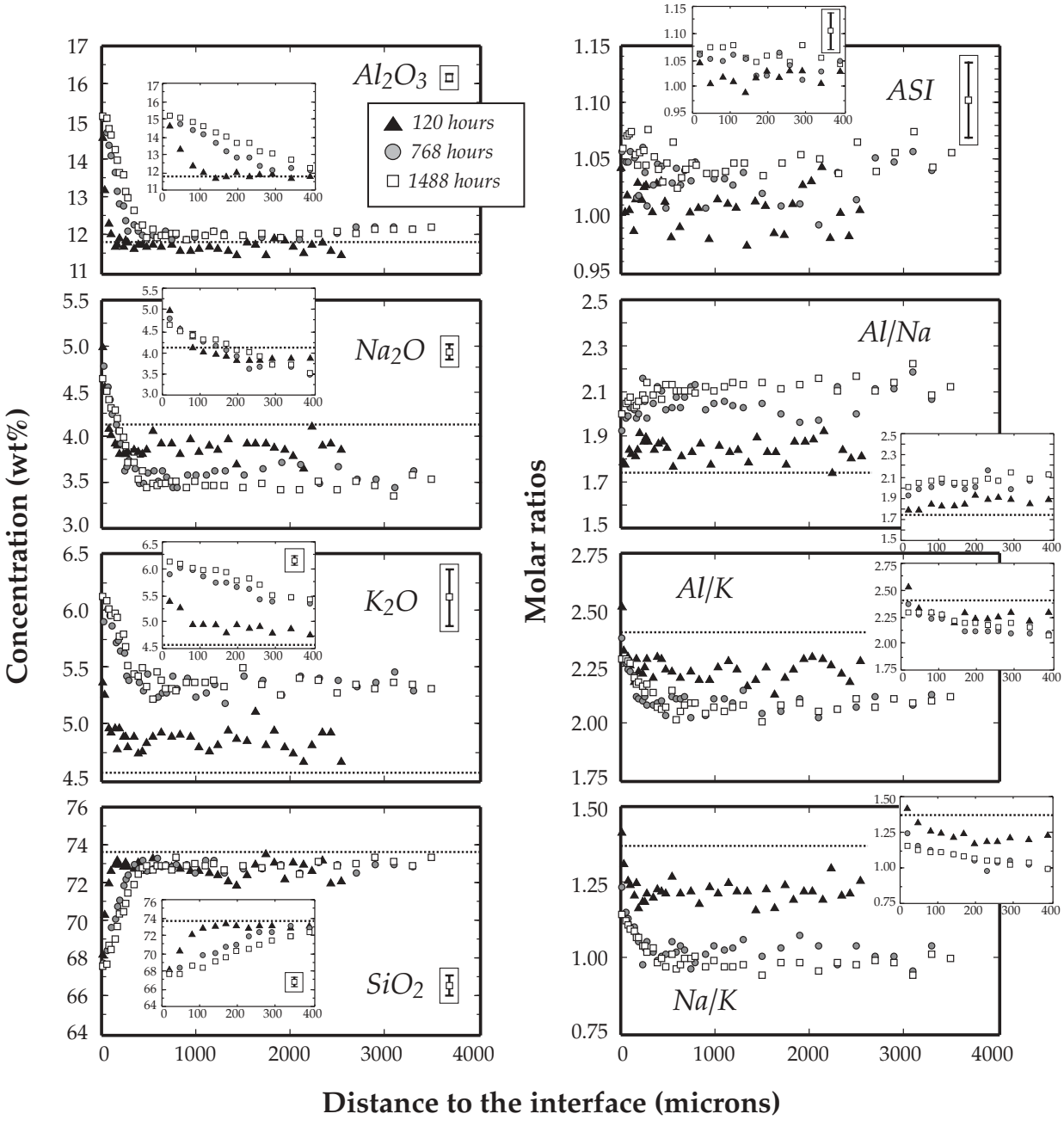


**Fig. 6.** Composition of glasses in the orthoclase dissolution experiments as a function of experimental time and distance to the orthoclase–glass interface.

mineral dissolution. A study of $H_2O$ diffusion (Acosta-Vigil *et al.*, 2005) showed that cylinders of the starting dry haplogranite glass ≈3·5 mm in diameter and 4–6 mm long (larger than in the current study) are completely hydrated and compositionally homogeneous after 48–60 h at the current run conditions. After 69 h of reaction in orthoclase dissolution experiment Acasi 286 (Table 2), glass farther than 30–50 μm from the mineral–melt interface is homogeneous (concentration profiles are flat) and compositionally identical to the starting hydrated glass CG 1 (Tables 1 and 2, Fig. 8a). This demonstrates that dissolution of orthoclase was just beginning after about 69 h, an experimental duration longer than that required for complete hydration–melting of the glass cylinders. Therefore, mineral dissolution in the current experiments is initiated in homogeneous, hydrous liquid.

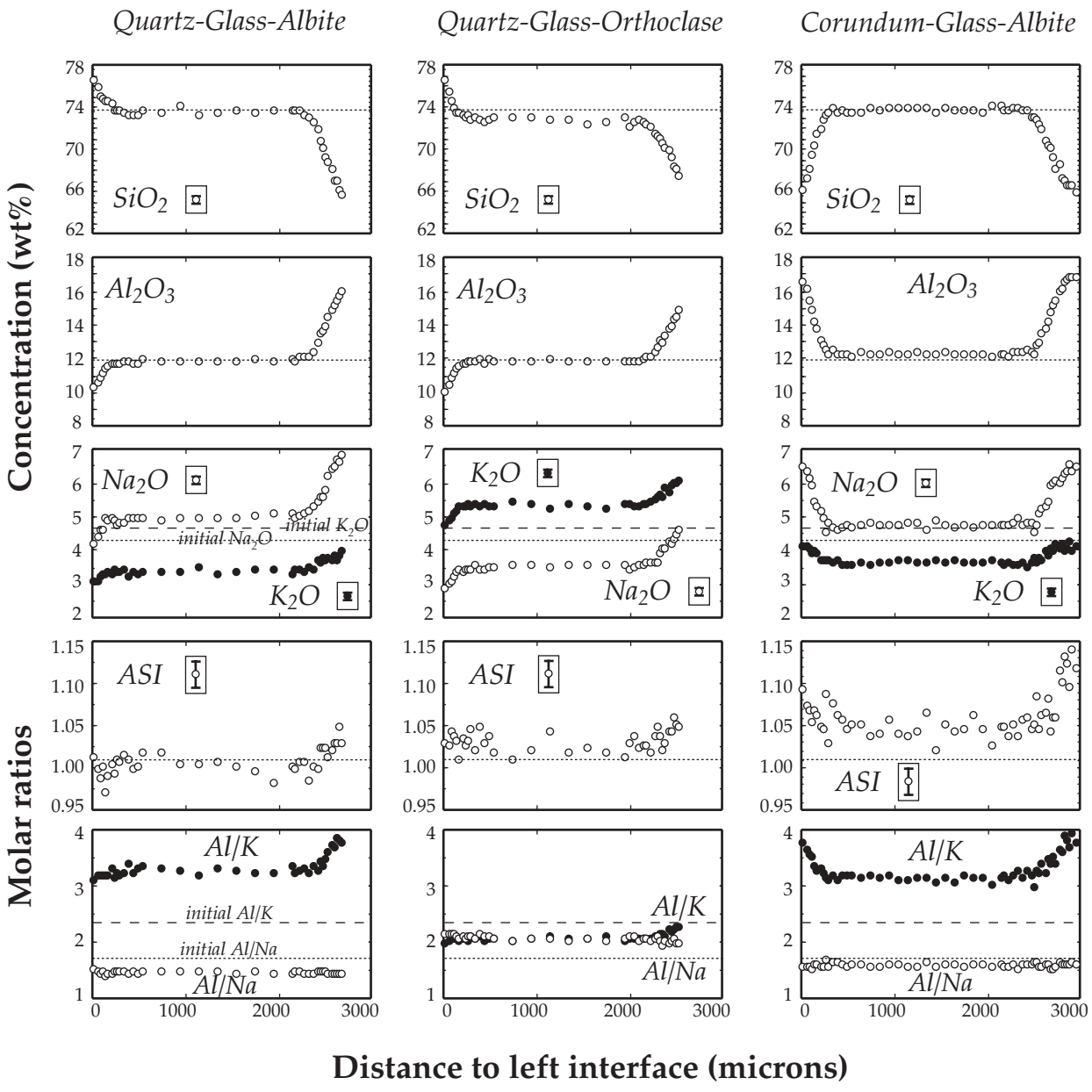


**Fig. 7.** Composition of glasses sandwiched between two mineral phases, as a function of distance to one of the interfaces. The nature and disposition of the mineral phases with respect to the glass are indicated at the top of the figure; for instance 'Quartz–Glass–Albite' means quartz to the left and albite to the right of the compositional profiles.

During initial cold pressurization of capsules, the gold or platinum tubes collapse around the length of the cores, squeezing almost all of the added water to strain shadows at the ends of the capsule. After hydration–melting of the glass cores, there is about 4–5 wt % free $H_2O$ fluid inside the capsule in contact with the mineral and melt cylinders. To verify that oxide concentration profiles in glass were produced only by dissolution of the mineral phase into melt at the interface and transport of components through the liquid, and was not influenced by lateral diffusion from the sides of the melt column via an aqueous vapor film, we conducted a 384 h orthoclase dissolution experiment using a glass core previously hydrated at the experimental conditions (Acasi 292, Table 2). An additional 1 wt % water was added to the capsule to keep the melt just at $H_2O$ saturation. Concentration profiles produced in this experiment are functionally identical to those in a 384 h orthoclase dissolution experiment starting with an anhydrous glass core. Small differences in $K_2O$ and Al/K profiles (Fig. 8b) are explained by the

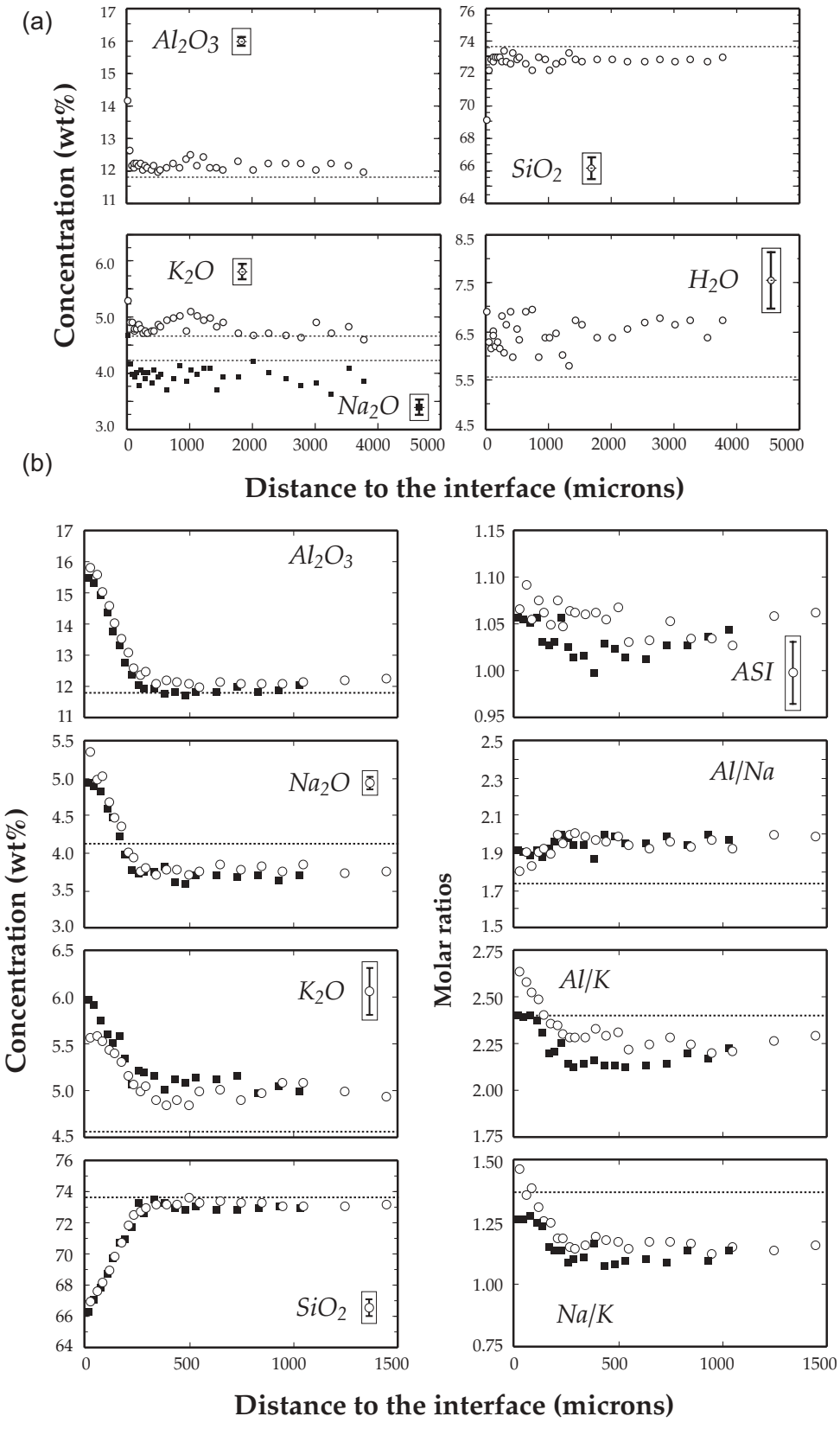

different lengths of starting glass cores (the starting anhydrous core being slightly shorter, implying a smaller volume for K diffusion as compared with the prehydrated core). Otherwise the behavior in both experiments is exactly the same, with aluminum diffusing about 250 μm away from the interface, sodium diffusing toward the interface throughout the entire melt reservoir to maintain a constant Al/Na ratio, and K diffusing away from the interface to maintain a constant ASI throughout the melt column. No irregular concentration profiles corresponding to sidewall diffusion from the melt–capsule interface were found in the current experiments [compare with fig. 2 of Acosta-Vigil *et al.* (2002) and relevant discussion]. These observations confirm that neither an excess $H_2O$ fluid phase in the capsule nor starting with anhydrous glass cylinders has any effect on the resultant concentration profiles in experimental glasses.

## ORIGIN OF THE CONCENTRATION PROFILES IN EXPERIMENTAL GLASSES

There are three main processes that potentially can govern the concentration profiles of melt components during the dissolution of a mineral phase into the melt: (1) the interface reaction or process by which mineral components detach from the mineral surface to enter the melt; (2) the diffusion of components through the melt; (3) convection in the melt (e.g. Donaldson, 1985; Zhang *et al.*, 1989). Convection did not occur or was not significant in these experiments because: (1) the concentrations of the oxide components in the glasses vary monotonically with the distance from the mineral–melt interface (compare with Shaw, 2000); (2) with increasing time the width of the melt boundary layer increases whereas the mineral dissolution rate decreases [Table 2 and Fig. 2; compare with Watson (1982)]. There are three conditions to be fulfilled for the profiles to be solely controlled by diffusion in the melt: (1) the composition of the interface melt is at the liquidus of the dissolving mineral phase at the conditions of the experiments; (2) the retreat of the mineral–melt interface is proportional to the square root of time; (3) the concentration profiles overlap when plotted against distance normalized to the square root of time (e.g. Crank, 1975; Zhang *et al.*, 1989; Liang, 1999). Regarding condition (1), Fig. 3 shows that after 384 h the interface melts are located very close to the liquidus surfaces of quartz and feldspars. Figure 2 shows that condition (2) is reasonably satisfied after 384 h of experimental time. Figure 9 shows that condition (3) also seems to hold after 384 h. However, we call attention to the observation that concentration profiles in albite and orthoclase dissolution experiments cannot rigorously overlap when plotted against distance normalized to time, because of the uphill diffusion of melt components throughout the entire melt column and the finite nature of the melt reservoir. Condition (3) seems to hold only for the case of semi-infinite melt reservoirs (see Acosta-Vigil *et al.*, 2002). We conclude that concentration profiles in the current experiments are controlled both by the kinetics of the interface reaction and diffusion in melt during an initial period of ≈240–384 h, but solely by diffusion of components in melt afterwards. Therefore, concentration profiles in experiments with durations ≥384 h can be reasonably described mathematically in terms of chemical diffusion in a multicomponent system.

## MULTICOMPONENT DIFFUSION MODELING

### General approach

A background on multicomponent chemical diffusion can be found elsewhere (e.g. Trial & Spera, 1994; Chakraborty, 1995). The current modeling aims to elucidate all or part of the diffusion matrix, **D**. The matrix **D** contains information about the directions in composition space along which diffusion is uncoupled (eigenvectors of **D**, $\gamma_i$), and the diffusivities along these directions (eigenvalues of ***D***, $\lambda_i$) at the given $P$–$T$–$X$ conditions (e.g. Chakraborty, 1995). Our approach to gain information about the eigenvectors is different from previous ones. Previous studies have used results from diffusion couple experiments (or isothermal interdiffusion experiments; Trial & Spera, 1994) for determining the entire diffusion matrix in silicate liquids (e.g. Kress & Ghiorso, 1993; Chakraborty *et al.*, 1995*a*; Liang *et al.*, 1996; Mungall *et al.*, 1998). Rather than diffusion couples, we began with dissolution experiments utilizing phases that contain only a single oxide component: corundum (Acosta-Vigil *et al.*, 2002), quartz (this work), and $H_2O$ (Acosta-Vigil *et al.*, 2005). This approach produces relatively simple concentration profiles in the melt because diffusion occurs mainly along the single uncoupled direction that is responsible for the diffusive transport of the oxide component ($SiO_2$, $Al_2O_3$, $H_2O$) added to the interface melt. Therefore, information about individual directions of uncoupled diffusion in the system can be obtained

**Fig. 8.** (a) Comparison between the compositions of the hydrated starting glass (CG 1, dashed lines) and the 69 h orthoclase dissolution experimental glass along profiles perpendicular to the interface (Acasi 286, ○, ■). (b) Comparison between the compositions of two 384 h orthoclase dissolution experiments, one starting with a hydrated glass cylinder (Acasi 292, ○), the other starting with a dry glass cylinder and excess water in the capsule (Acasi 232, ■).

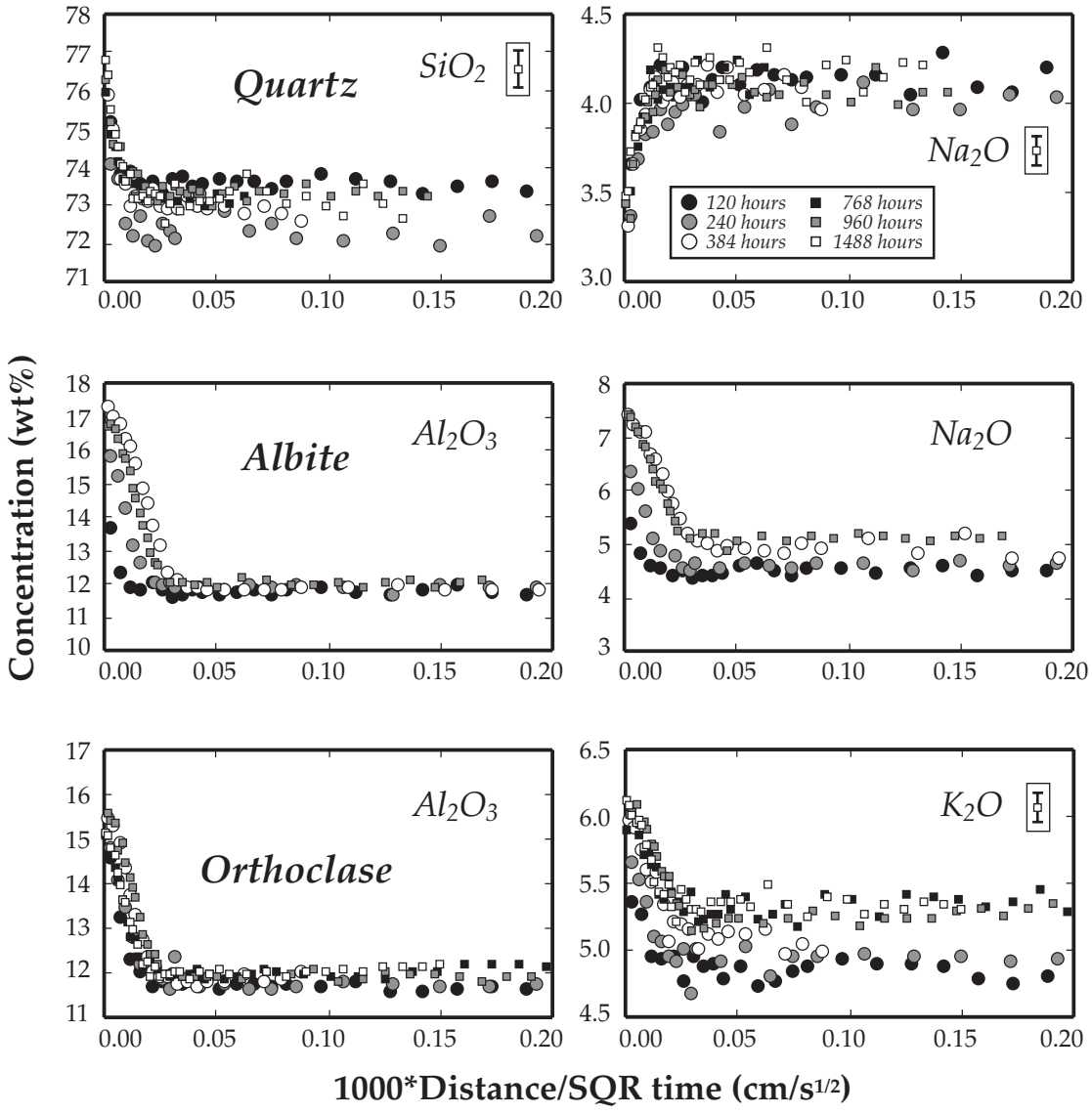


**Fig. 9.** Concentration of oxide components as a function of time and distance to the mineral–glass interface normalized to the square root of time, in glasses of the quartz, albite, and orthoclase dissolution experiments.

directly from the study of experimental concentration profiles. Diffusion data along additional directions of uncoupled diffusion in compositional space are then derived by dissolution of more complex mineral phases (e.g. feldspars: this work), each of which adds only one new component (e.g. K or Na) to the previously defined system. In this manner, diffusion data for all of the principal components in the granitic system can be derived from a succession of glass hydration–melting and single-mineral dissolution experiments. These results can be tested and verified afterward via additional complex mineral dissolution experiments (e.g. Acosta-Vigil *et al.*, 2002) or with sandwiched glass experiments (this work). In a system with $\mathcal{N}$ components, $\mathbf{D}$ is an $\mathcal{N}-1$ by $\mathcal{N}-1$ matrix, and the number of linearly independent eigenvectors is $\mathcal{N}-1$, each of them with an associated eigenvalue. The eigenvectors represent a new set of chemical components whose fluxes are independent of each other (e.g. Chakraborty, 1995). Each eigenvector is related to any other set of chemical components (e.g. oxide components) by $\mathcal{N}-1$ coefficients, which specify the proportions of the old components (oxides) in that particular eigenvector. $\mathbf{P}$ is an $\mathcal{N}-1$ by $\mathcal{N}-1$ matrix made of the eigenvector coefficients arranged in columns. For instance, $P_{ij}$ is a coefficient of $\mathbf{P}$ that refers to the proportion of the old component $i$ in the eigenvector $j$. As eigenvectors represent directions of uncoupled diffusion, these coefficients refer to the relative amounts of old

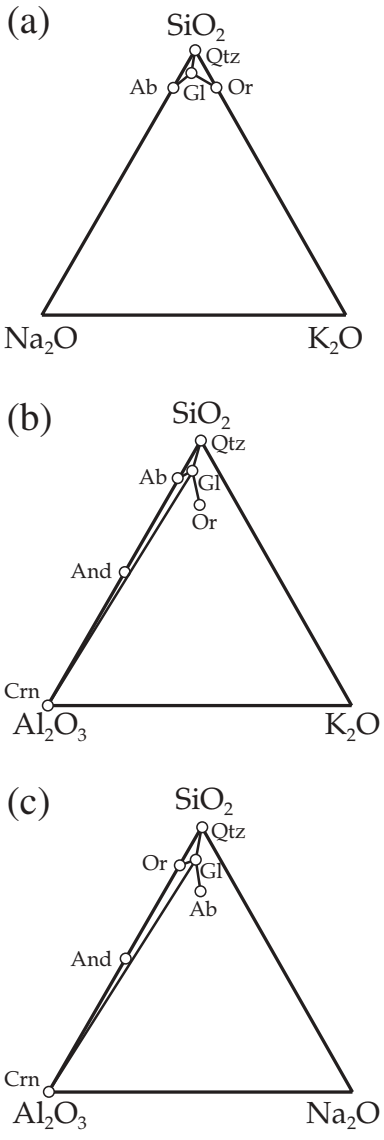


**Fig. 10.** Location in composition space (wt %) of the starting melt (Gl) and mineral phases used in the current experiments, projected from (a) $H_2O$ and $Al_2O_3$, (b) $H_2O$ and $Na_2O$, or (c) $H_2O$ and $K_2O$. Mineral symbols are taken from Kretz (1983).

components migrating at the same time and speed (see also Mungall *et al.*, 1998). We rely on this observation to gain information on the eigenvectors (matrix **P**) from the analysis of the oxide concentration profiles. Finally, to elucidate the eigenvalues of **D** we inverted the concentration profiles in melt produced by diffusion along three directions in composition space: quartz–, albite–, and orthoclase–water-saturated metaluminous haplogranite (Fig. 10). The procedure has been used previously (e.g. Trial & Spera, 1994; Mungall *et al.*, 1998; Acosta-Vigil *et al.*, 2002) and the reader is referred to these publications for a detailed explanation. During inversion of concentration profiles we used the information gained on the eigenvectors as additional constraints.

## Eigenvectors of D: constraints from compositional profiles

Quartz dissolution experiments show that neither aluminum nor alkalis are coupled with the diffusion of silica, because incorporation of silica into the melt produces proportionate dilution of the other components (compare with Sato, 1975; Watson, 1982; Chekhmir & Epel'baum, 1991; Shaw, 2000; Acosta-Vigil *et al.*, 2002). The collinearity of starting hydrous melt, quartz, and melt compositions from the boundary layers of all the quartz dissolution experiments demonstrates this conclusion (Fig. 11). In contrast, moderate coupling of CaO with $SiO_2$ in the system $CaO–Al_2O_3–SiO_2$ at 1500°C and 1 GPa produces compositions of bulk and boundary layer melts that are not collinear with quartz (Liang, 1999, fig. 5). Therefore, the coefficients of **P** associated with $\gamma_{Si}$ (the direction in composition space along which silica migrates to erase its concentration gradients), referenced to a six-oxygen oxide component stoichiometry, are $P_{AlSi} \approx 0$, $P_{NaSi} \approx 0$, $P_{KSi} \approx 0$, and $P_{SiSi} = 1$ (Table 5).

Feldspar dissolution experiments show that the migration of alkalis through melt does not require concomitant migration of silicon or aluminum; hence, neither silicon nor aluminum is coupled with the diffusion of alkalis. Although Na and K diffuse in the same direction during the dissolution of corundum and andalusite (Acosta-Vigil *et al.*, 2002), these components diffuse in opposite directions in the current feldspar dissolution experiments at the same *P–T–X* conditions, suggesting that Na and K can diffuse independently of each other. The coefficients for $\gamma_K$ are $P_{AlK} \approx 0$, $P_{NaK} \approx 0$, $P_{KK} \approx 1$ and $P_{SiK} \approx 0$, and those for $\gamma_{Na}$ are $P_{AlNa} \approx 0$, $P_{NaNa} \approx 1$, $P_{KNa} \approx 0$ and $P_{SiNa} \approx 0$ (Table 5).

Feldspar dissolution experiments also show that the migration of aluminum through melt requires concomitant migration of alkalis and, therefore, sodium and potassium are coupled with the diffusion of aluminum. The constant Al/Na molar ratio throughout the entire melt column at any experimental time implies that sodium is coupled with aluminum during diffusion along $\gamma_{Al}$, and that the relative molar amounts of Al and Na diffusing together are equal to the molar Al/Na ratio in the bulk melt (boundary layer + rest of melt cylinder). The constant ASI throughout the entire melt reservoir, equal to the ASI of melt at equilibrium, implies that potassium is also coupled with aluminum, and that the amount and direction of potassium diffusing with aluminum (and sodium) is such that the molar ratio Al/(Na + K) of this diffusing component is equal to the ASI of melt at equilibrium (see Fig. 12a). Following the previous observations we derive the following coefficients

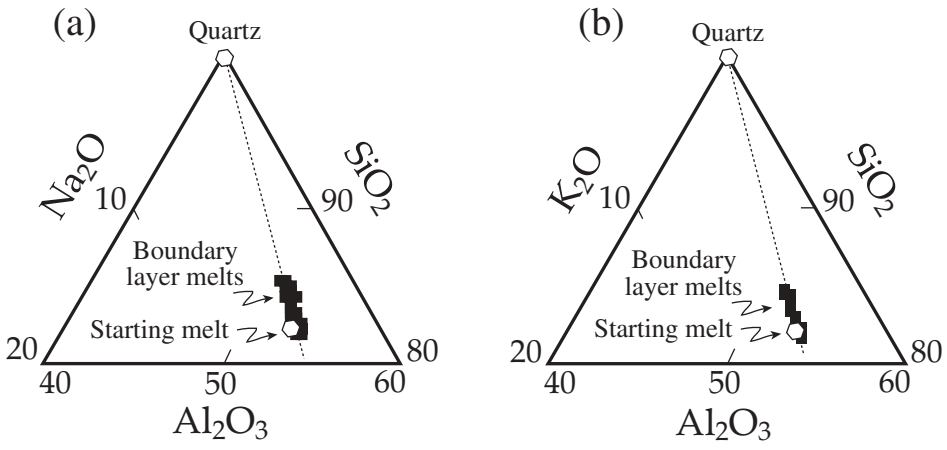


**Fig. 11.** Composition of starting hydrated melt and all analyses of glass (wt %) in the boundary layers of quartz dissolution experiments, projected from (a) $H_2O$ and $K_2O$, or (b) $H_2O$ and $Na_2O$. (See text for details.)

*Table 5: Eigenvectors coefficients (**P** matrix) deduced from analysis of the concentration profiles and referred to six-oxygen oxide components with $H_{12}O_6$ as solvent*

| | $P_{i\mathrm{Al}}$ | $P_{i\mathrm{Na}}$ | $P_{i\mathrm{K}}$ | $P_{i\mathrm{Si}}$ |
|---|---|---|---|---|
| $P_{\mathrm{Al}j}$ | 1 | 0 | 0 | 0 |
| $P_{\mathrm{Na}j}$ | 0·184 | 1 | 0 | 0 |
| $P_{\mathrm{K}j}$ | 0·142 | 0 | 1 | 0 |
| $P_{\mathrm{Si}j}$ | 0 | 0 | 0 | 1 |

for $\gamma_{\mathrm{Al}}$ (always referenced to the six-oxygen oxide component stoichiometry): $P_{\mathrm{AlAl}} \approx 1$, $P_{\mathrm{NaAl}} \approx 0{\cdot}184$, $P_{\mathrm{KAl}} \approx 0{\cdot}142$ and $P_{\mathrm{SiAl}} \approx 0$ (Table 5).

The orientations of the eigenvectors are invariant properties of the system at fixed *P–T–X* conditions and, therefore, are independent of the compositional direction along which diffusion takes place (e.g. Chakraborty, 1995). Together with Acosta-Vigil *et al.* (2002), the directions of uncoupled diffusion described above have been derived from diffusion concentration profiles along four different directions that intersect at the starting glass composition, three of them at high angle (Fig. 10). In addition, melt concentration profiles in the metaluminous quartz–feldspar sandwiched glass experiments are comparable with those in the single-mineral experiments. This supports the validity of the inferred directions of uncoupled diffusion. The addition of corundum in the albite–corundum sandwiched glass experiment makes the system peraluminous, and consequently $\gamma_{\mathrm{Al}}$ has a slightly different stoichiometry with respect to the metaluminous system (Fig. 12b; see also Acosta-Vigil *et al.*, 2002).

## Eigenvalues of D: inversion of concentration profiles

The single-mineral dissolution experiments have been modeled using the solutions to the diffusion equations provided by Smith *et al.* (1955) [as described by Acosta-Vigil *et al.* (2002)] and Liang (1999). These solutions are appropriate for diffusive mineral dissolution into a semi-infinite melt reservoir, with the mineral–melt interface retreating at a constant velocity (Smith *et al.*, 1955) or proportionally through the dissolution parameter $\alpha$ to the square root of both time and the diffusivity of the slowest component in melt (Liang, 1999). These solutions are convenient to model the quartz dissolution experiments, but not entirely appropriate to model the feldspar experiments because melt in the latter constitutes a finite reservoir. Their application to the feldspar experiments, however, can provide a good estimate of the diffusivity along the Al-eigenvector (see Acosta-Vigil *et al.*, 2002). These solutions assume that diffusion takes place only in one direction in space, that **D** is constant for the range in compositions of the melt, and that the changes in melt density with composition are negligible. We chose a six-oxygen stoichiometry for the oxide components, and $H_{12}O_6$ as the solvent. The six-oxygen basis permits comparison with previous sources of similar data (e.g. Mungall *et al.*, 1998), but is otherwise an arbitrary choice. The following modeling strategy was observed: (1) we inverted simultaneously all the concentration profiles in glass obtained by dissolution of a single mineral at different run times; (2) the eigenvector directions were fixed according to the observations regarding the evolution of concentration profiles with time (Table 5); (3) $\lambda_{\mathrm{Si}}$ was calculated by applying the solutions to the quartz dissolutions runs with durations of $\geq$384 h; (4) $\lambda_{\mathrm{Al}}$ was calculated by inverting the concentration profiles from the albite

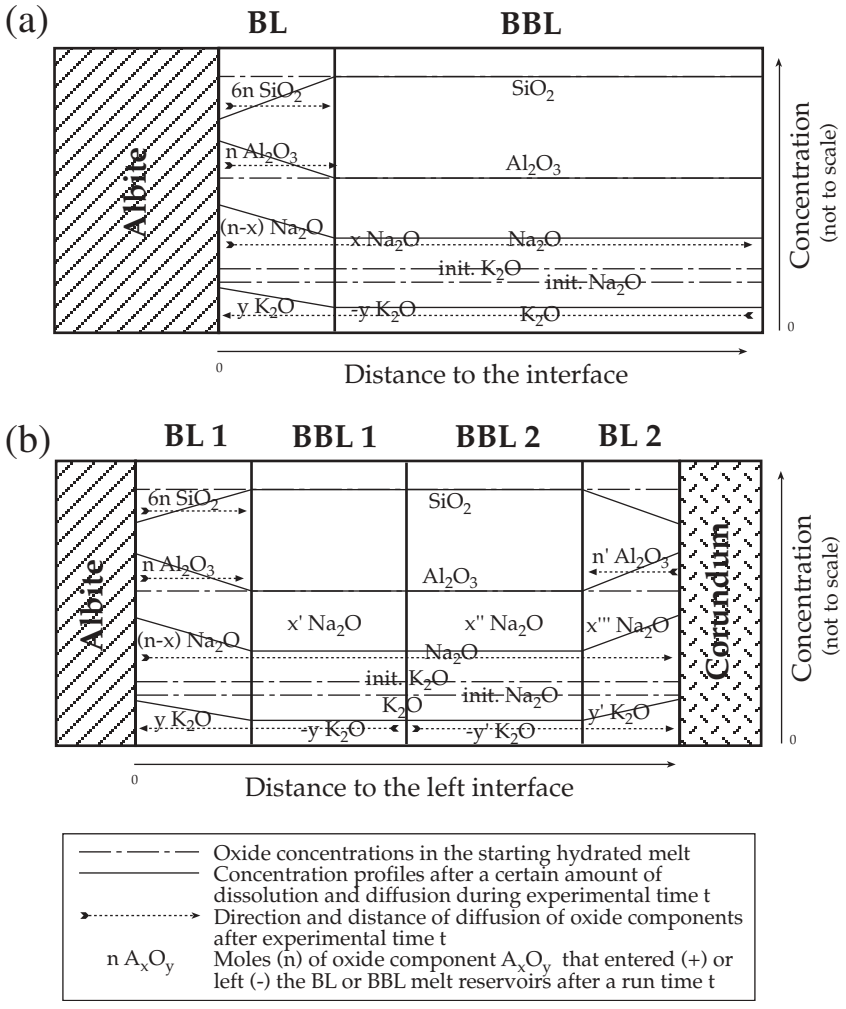


**Fig. 12.** (a) Schematic representation of an albite dissolution experiment showing starting and final oxide concentration profiles in the melt, and direction and distance of diffusion of the different oxide components. The melt column can be divided into two reservoirs: the volume within the boundary layer (BL) and the volume beyond the boundary layer (BBL). After an experimental time $t$, $2n$ moles of aluminum coming from albite have entered the BL melt reservoir. An equal molar amount of sodium has entered the melt too: a fraction of sodium atoms $2(n - x)$ remain in the BL and diffuse together with aluminum, whereas the rest ($2x$) decouple with respect to aluminum and migrate into the BBL reservoir in order to maintain a constant Al/Na molar ratio throughout the melt. Simultaneously, potassium diffuses uphill toward the interface: $2y$ moles of potassium leave the BBL reservoir and enter the BL reservoir to follow aluminum during its diffusion away from the interface. Because the ASI is roughly constant throughout the entire melt, the amount of sodium leaving BL and entering BBL, $2x$, is equal to the amount of potassium leaving BBL and entering BL, $y$. Therefore, the Al–Na–K diffusing component has an ASI ≈1 and its Al/Na molar ratio is that of the bulk system. (b) Schematic representation of the albite–glass–corundum sandwich experiment showing starting and final oxide concentration profiles in the melt, and direction and distance of diffusion of the different melt oxide components. The increase in ASI (Fig. 7) within the boundary layer next to the albite–glass interface (BL1) implies that the amount of sodium that decouples from aluminum and diffuses out of BL1 is greater than the amount of potassium migrating into BL1 to couple with aluminum. This means that the Al–Na–K diffusing component is peraluminous with an ASI of ≈1·15 or higher.

and orthoclase dissolution experiments with durations of ≥384 h.

The model results are presented in Table 6. Comparison between theoretical (Smith *et al.*, 1955) and experimental profiles for quartz, albite, and orthoclase dissolution experiments are shown in Fig. 13. Results for $\lambda_{Al}$ are similar to those obtained by Acosta-Vigil *et al.* (2002) using corundum dissolution experiments in the $H_2O$-saturated peraluminous haplogranite system at the same $P$–$T$ conditions. Although diffusivities for the alkalis were not obtained directly by the method described above, application of the equation $x^2 = Dt$ (e.g. Chakraborty, 1995) to data from Acosta-Vigil *et al.* (2002, 2005; this work) provides minimum chemical diffusivities of ≈(3–9) × $10^{-11}$ $m^2/s$ for sodium and potassium.

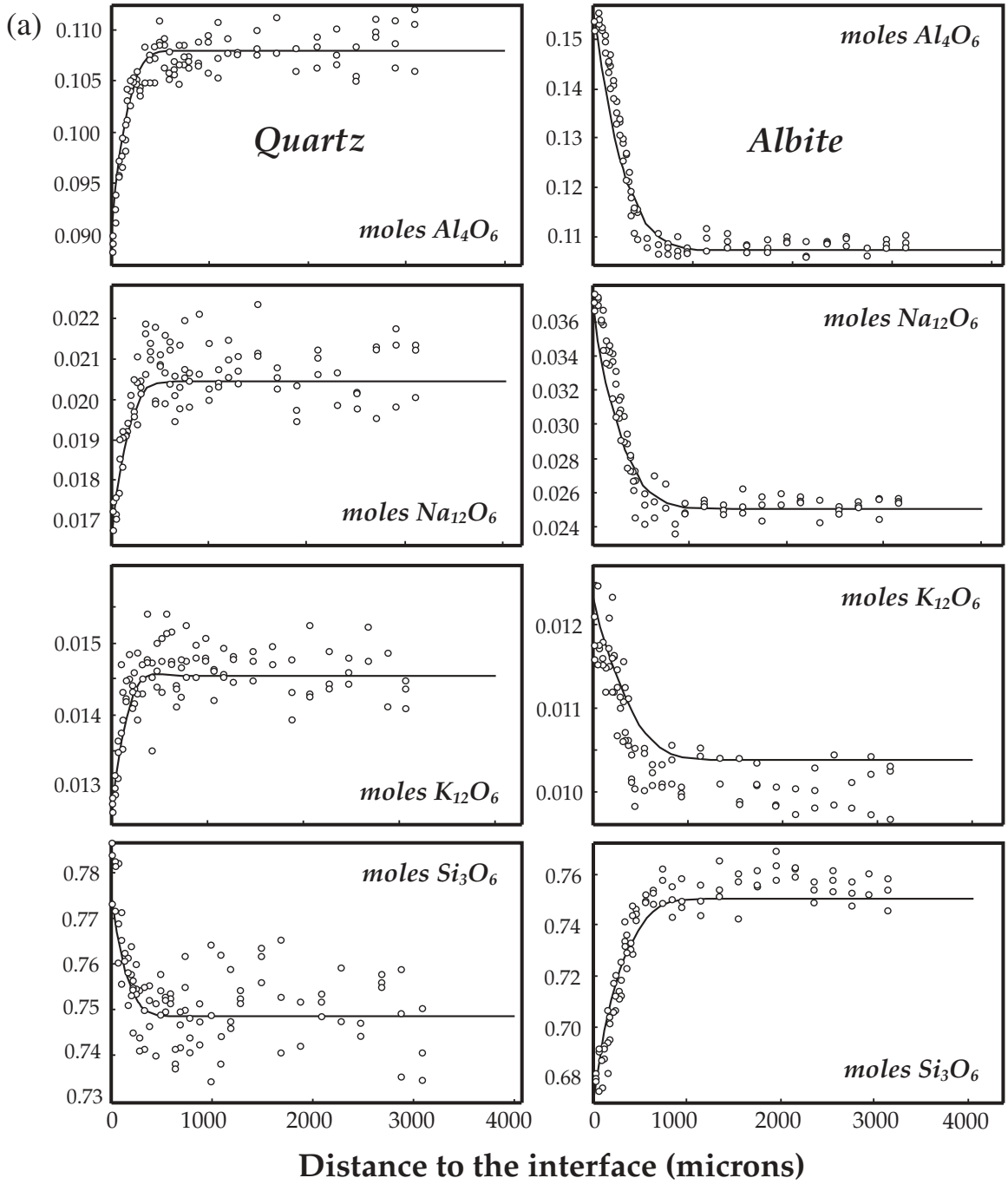


**Fig. 13.** Comparison between theoretical concentration profiles (lines) obtained with the solution by Smith *et al.* (1955) and eigenvectors and eigenvalues in Tables 5 and 6, and experimental profiles (○) for the 1488 h quartz dissolution experiment, 960 h albite experiment, and 1488 h orthoclase experiment.

## DISCUSSION

### Comparison with previous diffusion studies

Several studies of major element diffusion in granitic liquids (Watson, 1982; Baker, 1990, 1991; van der Laan & Wyllie, 1993) have provided effective binary diffusion coefficients (EBDC; Cooper, 1968) that are applicable to problems involving diffusion along the same directions of the diffusion couples in these experiments. They are not directly comparable with our diffusion coefficients, which are thought to represent diffusivities along chemical

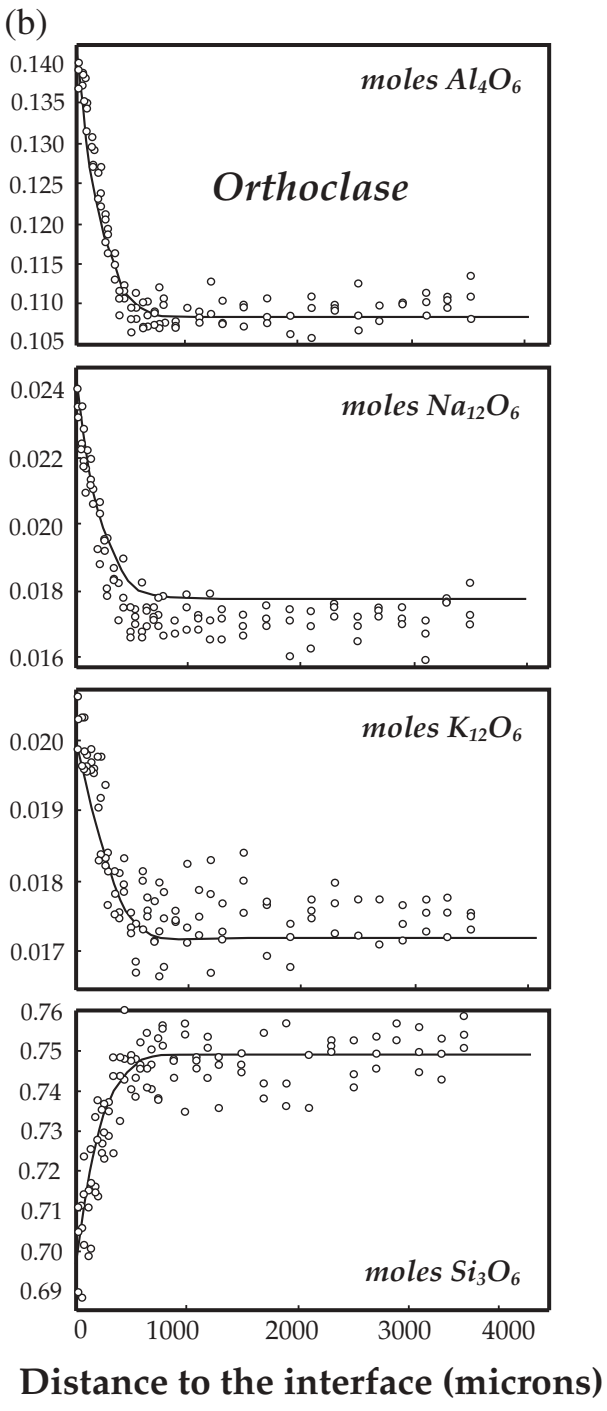


**Fig. 13.** *Continued.*

directions of uncoupled diffusion. Chakraborty *et al.* (1995*b*) found that in peralkaline and peraluminous portions of the system $K_2O$–$Al_2O_3$–$SiO_2$ at 1100–1600°C and 1 atm, diffusion of aluminum is coupled with a certain amount of potassium in the same direction, whereas diffusion of potassium does not involve migration of aluminum. These eigenvectors are in agreement with those obtained in the current study. Mungall *et al.* (1998) conducted diffusion couple experiments along several directions in composition space of the metaluminous $H_2O$-saturated haplogranite system at 1300–1600°C and 1 GPa, and also derived values for $\lambda_{Al}$ and $\gamma_{Al}$ comparable with our results (see also Acosta-Vigil *et al.*, 2002). Freda & Baker (1998) investigated the diffusion of Na and K between albite and orthoclase melts at 1200–1500°C, 1 GPa, and dry conditions. They observed that in the alkali feldspar system, alkalis interdiffuse independently of the other components. This is in accord with our observations in the $H_2O$-saturated haplogranite system, though we have also found that simultaneous migration of both alkalis can occur in either the same or opposite directions (Acosta-Vigil *et al.*, 2002). The diffusive transport properties of haplogranite melts do not vary from metaluminous to peraluminous systems (compare with Acosta-Vigil *et al.*, 2002). These similarities in the diffusion properties of a system at different pressure and temperature, or among systems with slightly different composition, are consistent with previous observations in the ternary $K_2O$–$Al_2O_3$–$SiO_2$ and $CaO$–$Al_2O_3$–$SiO_2$ systems, which showed only a small dependence of the eigenvector directions on pressure and temperature (Chakraborty *et al.*, 1995*a*, 1995*b*; Liang *et al.*, 1996, and references therein) or composition (peralkaline to peraluminous, Chakraborty *et al.*, 1995*a*, 1995*b*). However, the stoichiometry of eigenvectors can be appreciably different in systems of very different composition. For instance, several workers (Sato, 1975; Watson, 1982; Donaldson, 1985; Chekhmir & Epel'baum, 1991; Shaw, 2000) have found that potassium and sodium diffuse toward $SiO_2$-rich environments (e.g. as a result of dissolution of quartz) in basaltic systems, which we did not observe in our experiments. Such differences from the current study probably reflect significant changes in the coordination environments of elements and, hence, structure of the melt.

## Interaction between $H_2O$ and haplogranite components

Experimental data presented in this paper and by Acosta-Vigil *et al.* (2002, 2003, 2005) indicate that $H_2O$ in haplogranitic melts interacts preferentially with sodium and aluminum rather than with silicon and potassium. The concentration of $H_2O$ in melt seems to increase toward the mineral–melt interfaces in the corundum and several albite dissolution experiments, whereas it remains approximately constant in quartz and orthoclase dissolution experiments (Fig. 14a and b). This is in accordance with the observation by Holtz *et al.* (1992*a*, 1995), Behrens (1995), and Romano *et al.* (1996) that $H_2O$ solubility increases with the Na/K ratio of the melt, and with a growing body of experimental evidence

*Table 6: Eigenvalues calculated for the Si- and Al-eigenvectors with the solutions provided by Smith* et al. *(1955) and Liang (1999)*

| Experiments | Dissolution rate ($\times10^{-11}$ m/s) | Alpha parameter | Si-eigenvector Smith *et al.* (1955) ($\times10^{-15}$ m/s) | $\chi^2$ | Al-eigenvector Smith *et al.* (1955) ($\times10^{-14}$ m/s) | $\chi^2$ | Si-eigenvector Liang (1999) ($\times10^{-15}$ m/s) | $\chi^2$ | Al-eigenvector Liang (1999) ($\times10^{-14}$ m/s) | $\chi^2$ |
|---|---|---|---|---|---|---|---|---|---|---|
| Qtz dissolution | 0·015 | −0·020 | 2·8 | 0·0142 | | | 2·0 | 0·0159 | | |
| Ab dissolution | 4·051 | −0·011 | | | 2·4 | 0·0349 | | | 2·0 | 0·0380 |
| Or dissolution | 1·736 | −0·007 | | | 0·9 | 0·0300 | | | 0·6 | 0·0286 |

The goodness of the fit between model and experimental data is shown by the $\chi^2$ function. Mineral symbols are taken from Kretz (1983).

pointing to an association of excess aluminum and $H_2O$ or its dissociated components in granitic melts. For instance, various experimental studies have revealed that the capacity of granitic melts to dissolve $H_2O$ increases with their excess alumina concentration (Dingwell *et al.*, 1984, 1997; Holtz *et al.*, 1992*b*; Linnen *et al.*, 1996; Behrens & Jantos, 2001; Acosta-Vigil *et al.*, 2002). Mungall *et al.* (1998) deduced a slight coupling of hydrogen to aluminum during diffusion in $H_2O$-saturated haplogranite melt. Acosta-Vigil *et al.* (2003) have shown that $H_2O$ plays an essential role in dissolving excess alumina in granitic melts (see also Clemens & Wall, 1981; Patiño Douce, 1992; Dingwell *et al.*, 1997). Hence, excess aluminum and sodium seem to decrease the activity of $H_2O$ in granitic melt, suggesting that $H_2O$ or its dissociated components interact preferentially with these elements compared with silica and potassium. These observations can be relevant to the mechanisms of $H_2O$ dissolution in granitic melts (e.g. Schmidt *et al.*, 2000; Zeng *et al.*, 2000).

## Diffusion of group IA cations

In accordance with previous studies on diffusion in silicate (basaltic to granitic) melts at higher temperatures and variable pressures (1200–1600°C, 0·001–10 kbar: Watson, 1982; Baker, 1990; Mungall *et al.*, 1998), we find that chemical diffusion of alkalis is much faster (at least ≈3–4 orders of magnitude) than diffusion of the tetrahedral components of melt. There is a difference, however, in the behaviour of group IA cations during tracer vs chemical diffusion. Tracer diffusivities for group IA cations generally decrease with increasing atomic number, and hence with increasing ionic radius and mass; this occurs at a variety of dry glass and melt compositions, temperatures, and pressures (Jambon & Carron, 1973, 1976; Jambon, 1982; Lowry *et al.*, 1982; Henderson *et al.*, 1985). Our diffusion studies in wet haplogranite liquids at 800°C (Acosta-Vigil *et al.*, 2002, 2005; this work) show, however, that chemical diffusivities for sodium and potassium are comparable with, and at least of the same magnitude as those for hydrogen ($\approx10^{-11}$–$10^{-10}$ $m^2/s$). In agreement with this, Mungall *et al.* (1998) have found that calculated eigenvalues for $\gamma_{Na}$, $\gamma_K$, and $\gamma_H$ at 1600°C are degenerate within the precision of their experimental data. This indicates that at least for the particular case of group IA cations and wet haplogranite melts, chemical diffusivity does not depend primarily on ionic volume or mass. These differences are probably due to the different nature of (and possibly different diffusion mechanisms involved in) tracer vs chemical diffusion (e.g. see Hofmann, 1980; Dunn, 1986). Finally, we note that compared with potassium, sodium has a special role in charge-balancing aluminum (Acosta-Vigil *et al.*, 2002; this work). This is shown by the constant Al/Na molar ratio during the existence of Al gradients in melt. This does not seem to be due to differences in diffusivities; it is more likely to be produced by differences in the coordination environments, perhaps related to the energetics of their bonds (Acosta-Vigil *et al.*, 2005).

## Large-scale effects of chemical diffusion

Since the work of Bowen (1921), it has been largely considered that chemical diffusion is not an effective process for modifying the composition of silicate liquids on a large scale in the time frame of magmatic processes [see reviews by Hofmann (1980) and Watson (1994)]. This may not be entirely true, however, regarding diffusion of sodium and potassium. Rather than the calculated diffusivities, the important observation here is that diffusion of alkalis can be extremely rapid when associated with the diffusion of aluminum; that is, when aluminum concentration gradients are present in the melt, sodium migrates instantaneously (compared with the time frame of the experiments) to maintain a constant Al/Na molar ratio throughout the entire melt reservoir, whereas K diffuses concomitantly and at the same rate in the direction needed to maintain or achieve the ASI of

equilibrium (Acosta-Vigil *et al.*, 2002; this work). The increase in ASI toward albite in the peraluminous sandwiched glass experiment means that there is a long-range chemical communication in the melt through chemical potential gradients that tend to be erased by the high diffusivity of the alkali elements. Acosta-Vigil *et al.* (2004, and unpublished data) have found that during the $H_2O$-saturated partial melting of leucogranite cylinders 3·5 mm in diameter and 7 mm in length, at 200 MPa and 690–800°C, granitic melt distributed throughout the entire cylinder possesses constant Al/Na and ASI molar ratios at any experimental time, from 11 to 2925 h, even though variations in Al/Si may persist.

## Geological applications

Diffusion is a major process controlling the chemical composition of silicate liquids during anatexis, magma mixing, assimilation, or crystallization. The wet haplogranite system under investigation here makes up 95–99 wt % of natural, restite-free granitic magmas. The experimental results presented in this work, therefore, have applications for predicting the composition of granitic liquids during these geological processes. Given an appropriate solution to the diffusion equations for a particular geological situation (e.g. Crank, 1975), application of diffusivities along directions of uncoupled diffusion will provide melt composition at a given time and distance with respect to a reference frame. These results also are relevant to interpreting the chemistry of glass inclusions trapped during crustal anatexis (Cesare *et al.*, 1997, 2003). An important reason for the present study was to gain information about the rates at which crustal granitic melts can be produced, how homogeneous they are, and how much time it takes for them to achieve homogenization. As an example, a similar experimental program involving the dissolution of corundum into metaluminous granitic melt led to an estimate for the time required to reach the equilibrium composition of melt for a specific scenario of corundum grains dispersed in a quartzofeldspathic rock (Acosta-Vigil *et al.*, 2002). Diffusion is not the only process that may control the production of melt; the rate of heat supply is also very important and, in many cases, is the rate-limiting factor (e.g. Rubie & Brearley, 1990). Shear during deformation or viscous flow of magma may also promote the homogenization of melts, but diffusion will operate none the less. The application of this work, therefore, could be considered as a component of a more complex problem, or could be modeled as a specific scenario. That scenario could be one in which a

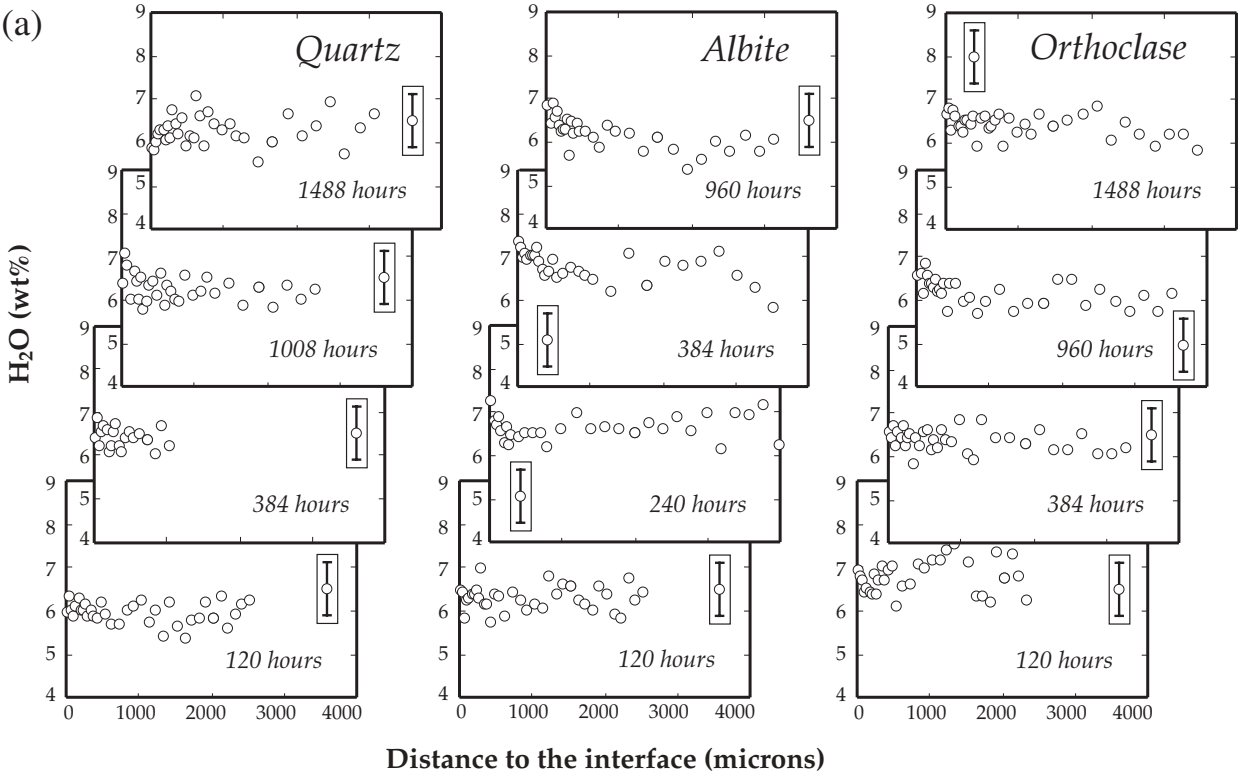


**Fig. 14.** (a) Glass $H_2O$ concentration calculated by difference in the quartz, albite, and orthoclase dissolution experiments, as a function of distance to the mineral–glass interface and experimental time. (b) $H_2O$ concentration in glasses of the sandwiched glass experiments as a function of distance to one of the interfaces. The nature and disposition of the mineral phases are indicated. Mineral symbols after Kretz (1983).

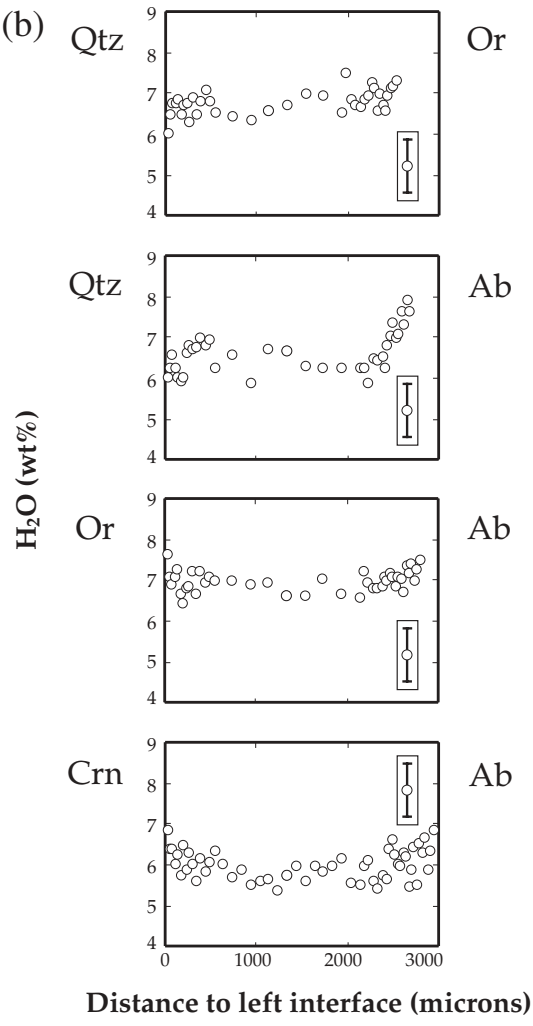


**Fig. 14.** *Continued.*

large mass of mafic liquid intrudes crustal quartzofeldspathic rocks that are vapor ($H_2O$) saturated along their grain boundaries. The temperature rises to $\geq$800°C in the quartzofeldspathic rocks along the margins of the mafic body, and the supply of heat is essentially infinite, albeit transient over the period of cooling. The conditions of this scenario have been recognized in anatectic settings on a small scale (e.g. Holness *et al.*, 2005), and they may also operate at the regional scale (e.g. Loomis, 1972). Under such conditions, our study indicates that crustal melting would be diffusion-controlled once mineral phases lose contact and each mineral dissolves at a rate governed by the diffusion of components in the melt. The diffusivity of the slowest-diffusing component in melt and the proportion of melting will determine the minimum duration of the melting event. The application of the equation $x^2 = Dt$ and the diffusivity determined for silica in this study indicates that 20–30 vol. % partial melting of a quartzofeldspathic rock with initial grain size of 2–3 mm (resulting in a mean distance of separation between restite grains of 250–500 μm) and homogenization of melt will take place in less than 1–10 years. This represents the maximum rate of crustal melting when diffusion is the only mechanism for mixing in the melt.

## SUMMARY AND CONCLUSIONS

The key observation of this work is the complex relationship among Al, Na, and K during diffusion of these components through haplogranitic melt along chemical potential gradients induced by crystal dissolution. When gradients in Al exist, Na diffuses instantaneously to achieve a constant molar Al/Na ratio everywhere in the melt, and K diffuses so as to achieve or maintain the ASI value of the melt at equilibrium. Diffusion of Si produces only dilution of the other components, and no interactions with them. The maximum rate at which quartz, plagioclase, and K-feldspar can melt at 800°C and under conditions of hydrostatic stress and $H_2O$ saturation is determined by the diffusivities of their components in the melt. When used in conjunction with appropriate solutions to the diffusion equations, these diffusivities constitute an important part of a solution to the duration of crustal melting events.

## ACKNOWLEDGEMENTS

Support for this research was provided by National Science Foundation grants EAR-990165, INT-9603199, EAR-9618867, EAR-9625517, EAR-9404658, and a postdoctoral grant to A.A.V. from the Universidad de Granada, Spain. The Electron Microprobe Laboratory at the University of Oklahoma was created with US DOE grant DE-FG22-87FE1146 and upgraded with NSF grant EAR-9404658 and support from the University of Oklahoma Office of Research Administration. We thank Don Baker, Alberto Patiño Douce, Dennis Geist and an anonymous referee for thorough reviews that improved greatly the consistency and clarity of the manuscript.

## REFERENCES

Acosta-Vigil, A., London, D., Dewers, T. A. & Morgan, G. B., VI (2002). Dissolution of corundum and andalusite in $H_2O$-saturated haplogranitic melts at 800°C and 200 MPa: constraints on diffusivities and the generation of peraluminous melts. *Journal of Petrology* **43**, 1885–1908.

Acosta-Vigil, A., London, D., Morgan, G. B., VI & Dewers, T. A. (2003). Solubility of excess alumina in hydrous granitic melts in equilibrium with peraluminous minerals at 700–800°C and 200 MPa, and applications of the aluminum saturation index. *Contributions to Mineralogy and Petrology* **146**, 100–119.

Acosta-Vigil, A., London, D. & Morgan, G. B., VI (2004). Composition and distribution of melt during partial melting of a leucogranite at 200 MPa $H_2O$. *Geological Society of America, Abstracts with Programs* **36**, 45.

Acosta-Vigil, A., London, D. & Morgan, G. B., VI (2005). Contrasting interactions of sodium and potassium with $H_2O$ in haplogranitic liquids and glasses at 200 MPa from hydration–diffusion experiments. *Contributions to Mineralogy and Petrology* **149**, 276–287.

Arzi, A. A. (1978). Fusion kinetics, water pressure, water diffusion and electrical conductivity in melting rocks, interrelated. *Journal of Petrology* **19**, 153–169.

Baker, D. R. (1990). Chemical interdiffusion of dacite and rhyolite: anhydrous measurements at 1 atm and 10 kbar, application of transition state theory, and diffusion in zoned magma chambers. *Contributions to Mineralogy and Petrology* **104**, 407–423.

Baker, D. R. (1991). Interdiffusion of hydrous dacitic and rhyolitic melts and the efficacy of rhyolite contamination of dacitic enclaves. *Contributions to Mineralogy and Petrology* **106**, 462–473.

Barbero, L., Villaseca, C., Rogers, G. & Brown, P. E. (1995). Geochemical and isotopic disequilibrium in crustal melting: an insight from the anatectic granitoids from Toledo, Spain. *Journal of Geophysical Research* **100**, 15745–15765.

Behrens, H. (1995). Determination of water solubilities in high-viscosity melts: an experimental study on $NaAlSi_3O_8$ and $KAlSi_3O_8$ melts. *European Journal of Mineralogy* **7**, 905–920.

Behrens, H. & Jantos, N. (2001). The effect of anhydrous composition on water solubility in granitic melts. *American Mineralogist* **86**, 14–20.

Bowen, N. L. (1921). Diffusion in silicate melts. *Journal of Geology* **29**, 295–317.

Brown, M., Averkin, Y. A., McLellan, E. L. & Sawyer, E. W. (1995). Mechanisms and consequences of melt segregation from crustal protoliths. *Journal of Geophysical Research* **100**, 15655–15679.

Büsch, W., Schneider, G. & Mehnert, K. R. (1974). Initial melting at grain boundaries. Part II: melting in rocks of granodioritic, quartzdioritic and tonalitic composition. *Neues Jahrbuch für Mineralogie, Monatshefte* **5**, 345–370.

Cesare, B., Salvioli Mariani, E. & Venturelli, G. (1997). Crustal anatexis and melt extraction during deformation in the restitic xenoliths at El Joyazo (SE Spain). *Mineralogical Magazine* **61**, 15–27.

Cesare, B., Marchesi, C., Hermann, J. & Gomez-Pugnaire, M.T. (2003). Primary melt inclusions in andalusite from anatectic graphitic metapelites: implications for the position of the $Al_2SiO_5$ triple point. *Geology* **31**, 573–576.

Chakraborty, S. (1995). Diffusion in silicate melts. In: Stebbins, J. F., McMillan, P. F. & Dingwell, D. B. (eds) *Structure, Dynamics and Properties of Silicate Melts. Mineralogical Society of America, Reviews in Mineralogy* **32**, 411–504.

Chakraborty, S., Dingwell, D. B. & Rubie, D. C. (1995*a*). Multicomponent diffusion in ternary silicate melts in the system $K_2O$–$Al_2O_3$–$SiO_2$: I. Experimental measurements. *Geochimica et Cosmochimica Acta* **59**, 255–264.

Chakraborty, S., Dingwell, D. B. & Rubie, D. C. (1995*b*). Multicomponent diffusion in ternary silicate melts in the system $K_2O$–$Al_2O_3$–$SiO_2$: II. Mechanisms, systematics, and geological applications. *Geochimica et Cosmochimica Acta* **59**, 265–277.

Chekhmir, A. S. & Epel'baum, M. B. (1991). Diffusion in magmatic melts: new study. In: Perchuk, L. L. & Kushiro, I. (eds) *Physical Chemistry of Magmas*. New York: Springer, pp. 99–119.

Clemens, J. D. & Wall, V. J. (1981). Origin and crystallization of some peraluminous (S-type) granitic magmas. *Canadian Mineralogist* **19**, 111–131.

Cooper, A. R., Jr (1968). The use and limitations of the concept of an effective binary diffusion coefficient for multicomponent diffusion. In: Wachtman, J. B., Jr & Franklin, A. D. (eds) *Mass Transport in Oxides. National Bureau of Standards Special Publication* **196**, 79–84.

Cooper, A. R., Jr & Kingery, W. D. (1964). Dissolution in ceramic systems: I, molecular diffusion, natural convection, and forced convection studies of sapphire dissolution in calcium aluminum silicate. *Journal of the American Ceramic Society* **47**, 37–43.

Crank, J. (1975). *The Mathematics of Diffusion*. Oxford: Clarendon Press.

Dingwell, D. B., Harris, D. M. & Scarfe, C. M. (1984). The solubility of $H_2O$ in melts in the system $SiO_2$–$Al_2O_3$–$Na_2O$–$K_2O$ at 1 to 2 kbars. *Journal of Geology* **92**, 387–395.

Dingwell, D. M., Holtz, F. & Behrens, H. (1997). The solubility of $H_2O$ in peralkaline and peraluminous granitic melts. *American Mineralogist* **82**, 434–437.

Donaldson, C. H. (1985). The rates of dissolution of olivine, plagioclase, and quartz in a basalt melt. *Mineralogical Magazine* **49**, 683–693.

Dunn, T. (1986). Diffusion in silicate melts: an introduction and literature review. In: Scarfe, C. M. (ed.) *Short Course in Silicate Melts. Mineralogical Association of Canada, Short Course Handbook* **12**, 57–92.

Freda, C. & Baker, D. R. (1998). Na–K interdiffusion in alkali feldspar melts. *Geochimica et Cosmochimica Acta* **62**, 2997–3007.

Gan, H. & Hess, P.C. (1992). Phosphate speciation in potassium aluminosilicate glasses. *American Mineralogist* **77**, 495–506.

Harris, N., Vance, D. & Ayres, M. (2000). From sediment to granite: timescales of anatexis in the upper crust. *Chemical Geology* **162**, 155–167.

Henderson, P., Nolan, J., Cunningham, G. C. & Lowry, R. K. (1985). Structural controls and mechanisms of diffusion in natural silicate melts. *Contributions to Mineralogy and Petrology* **89**, 263–272.

Hofmann, A. W. (1980). Diffusion in natural silicate melts: a critical review. In: Hargraves, R. B. (ed.) *Physics of Magmatic Processes*. Princeton, NJ: Princeton University Press, pp. 385–417.

Holness, M. B., Dane, K., Sides, R., Richardson, C. & Caddick, M. (2005). Melting and segregation in the aureole of the Glenmore Plug, Ardnamurchan. *Journal of Metamorphic Geology* **23**, 29–43.

Holtz, F., Behrens, H., Dingwell, D. B. & Taylor, R. P. (1992*a*). Water solubility in aluminosilicate melts of haplogranite composition at 2 kbar. *Chemical Geology* **96**, 289–302.

Holtz, F., Johannes, W. & Pichavant, M. (1992*b*). Peraluminous granites: the effect of alumina on melt composition and coexisting minerals. *Transactions of the Royal Society of Edinburgh: Earth Sciences* **83**, 409–416.

Holtz, F., Behrens, H., Dingwell, D. B. & Johannes, W. (1995). $H_2O$ solubility in haplogranitic melts: compositional, pressure, and temperature dependence. *American Mineralogist* **80**, 94–108.

Jambon, A. (1982). Tracer diffusion in granitic melt: experimental results for Na, K, Rb, Cs, Ca, Sr, Ba, Ce, Eu to 1300°C and a model of calculation. *Journal of Geophysical Research* **87**, 10797–10810.

Jambon, A. & Carron, J. P. (1973). Étude expérimentale de la diffusion des éléments alkalins K, Rb, Cs dans une obsidienne granitique. *Comptes Rendus de l'Académie des Sciences, Série D* **276**, 3069–3072.

Jambon, A. & Carron, J. P. (1976). Diffusion of Na, K, Rb and Cs in glasses of albite and orthoclase composition. *Geochimica et Cosmochimica Acta* **40**, 897–903.

Kress, V. C. & Ghiorso, M. S. (1993). Multicomponent diffusion in $MgO$–$Al_2O_3$–$SiO_2$ and $CaO$–$MgO$–$Al_2O_3$–$SiO_2$ melts. *Geochimica et Cosmochimica Acta* **57**, 4453–4466.

Kretz, R. (1983). Symbols for rock-forming minerals. *American Mineralogist* **68**, 277–279.

Lesher, C. E. (1994). Kinetics of Sr and Nd exchange in silicate liquids: theory, experiments, and applications to uphill diffusion, isotopic equilibration, and irreversible mixing of magmas. *Journal of Geophysical Research* **99**, 9585–9604.

Liang, Y. (1999). Diffusive dissolution in ternary systems: analysis with applications to quartz and quartzite dissolution in molten silicates. *Geochimica et Cosmochimica Acta* **63**, 3983–3995.

Liang, Y., Richter, F. M. & Watson, E. B. (1996). Diffusion in silicate melts: II. Multicomponent diffusion in $CaO$–$Al_2O_3$–$SiO_2$ at 1500°C and 1 GPa. *Geochimica et Cosmochimica Acta* **60**, 5021–5035.

Linnen, R. L., Pichavant, M. & Holtz, F. (1996). The combined effects of $fO_2$ and melt composition on $SnO_2$ solubility and tin diffusivity in haplogranitic melts. *Geochimica et Cosmochimica Acta* **60**, 4965–4976.

Loomis, T. P. (1972). Contact metamorphism of pelitic rocks by the Ronda ultramafic intrusion, Southern Spain. *Geological Society of America Bulletin* **83**, 2449–2474.

Lowry, R. K., Henderson, P. & Nolan, J. (1982). Tracer diffusion of some alkali, alkaline-earth and transition element ions in a basaltic and an andesitic melt, and the implications concerning melt structure. *Contributions to Mineralogy and Petrology* **80**, 254–261.

Mehnert, K. R., Büsch, W. & Schneider, G. (1973). Initial melting at grain boundaries of quartz and feldspar in gneisses and granulites. *Neues Jahrbuch für Mineralogie, Monatshefte* **4**, 165–183.

Morgan, G. B., VI & London, D. (1996). Optimizing the electron microprobe analysis of hydrous alkali aluminosilicate glasses. *American Mineralogist* **81**, 1176–1185.

Mungall, J. E., Romano, C. & Dingwell, D. B. (1998). Multicomponent diffusion in the molten system $K_2O$–$Na_2O$–$Al_2O_3$–$SiO_2$–$H_2O$. *American Mineralogist* **83**, 685–699.

Mysen, B. O., Ryerson, F. J. & Virgo, D. (1981). The structural role of phosphorus in silicate melts. *American Mineralogist* **66**, 106–117.

Mysen, B. O., Holtz, F., Pichavant, M., Beny, J. M. & Montel, J. M. (1999). The effect of temperature and bulk composition on the solution mechanism of phosphorus in peraluminous haplogranitic magmas. *American Mineralogist* **84**, 1336–1345.

Patiño Douce, A. E. (1992). Calculated relationships between activity of alumina and phase assemblages of silica-saturated igneous rocks. *Journal of Volcanology and Geothermal Research* **52**, 43–63.

Pouchou, J. L. & Pichoir, F. (1985). 'PAP' $\phi(\rho z)$ correction procedure for improved quantitative microanalysis. In: Armstrong, J. T. (ed.) *Microbeam Analysis*. San Francisco, CA: San Francisco Press, pp. 104–106.

Romano, C., Dingwell, D. B., Behrens, H. & Dolfi, D. (1996) Compositional dependence of $H_2O$ solubility along the joins $NaAlSi_3O_8$–$KAlSi_3O_8$, $NaAlSi_3O_8$–$LiAlSi_3O_8$, and $KAlSi_3O_8$–$LiAlSi_3O_8$. *American Mineralogist* **81**, 452–461.

Rubie, D. C. & Brearley, A. J. (1990). A model for rates of disequilibrium melting during metamorphism. In: Ashworth, J. R. & Brown, M. (eds) *High-temperature Metamorphism and Crustal Anatexis*. London: Unwin Hyman, pp. 57–86.

Sato, H. (1975). Diffusion coronas around quartz xenocrysts in andesite and basalt from Tertiary volcanic region in northeastern Shikoku, Japan. *Contributions to Mineralogy and Petrology* **50**, 49–64.

Sawyer, E. W. (1991). Disequilibrium melting and the rate of melt–residuum separation during migmatization of mafic rocks from the Grenville Front, Quebec. *Journal of Petrology* **32**, 701–738.

Schmidt, B. C., Riemer, T., Kohn, S. C., Behrens, H. & Dupree, R. (2000). Different water solubility mechanisms in hydrous glasses along the Qz–Ab join: evidence from NMR spectroscopy. *Geochimica et Cosmochimica Acta* **64**, 513–526.

Shaw, C. S. J. (2000). The effect of experiment geometry on the mechanism and rate of dissolution of quartz in basanite at 0·5 GPa and 1350°C. *Contributions to Mineralogy and Petrology* **139**, 509–525.

Shaw, C. S. J. (2004). Mechanisms and rates of quartz dissolution in melts in the CMAS ($CaO$–$MgO$–$Al_2O_3$–$SiO_2$) system. *Contributions to Mineralogy and Petrology* **148**, 180–200.

Smith, V. G., Tiller, W. A. & Rutter, J. W. (1955). A mathematical analysis of solute redistribution during solidification. *Canadian Journal of Physics* **33**, 723–745.

Taylor, J. R. & Wall, V. J. (1992). The behaviour of tin in granitoid magmas. *Economic Geology* **87**, 403–420.

Toplis, M. J. & Schaller, T. (1998). A $^{31}$P MAS NMR study of glasses in the system $xNa_2O$–$(1 - x)Al_2O_3$–$2SiO_2$–$yP_2O_5$. *Journal of Non-Crystalline Solids* **224**, 57–68.

Trial, A. F. & Spera, F. J. (1994). Measuring the multicomponent diffusion matrix: experimental design and data analysis for silicate melts. *Geochimica et Cosmochimica Acta* **58**, 3769–3783.

Tuttle, O. F. & Bowen, N. L. (1958). *Origin of Granite in the Light of Experimental Studies in the System $NaAlSi_3O_8$–$KAlSi_3O_8$–$SiO_2$–$H_2O$. Geological Society of America Memoir* **74**.

Van der Laan, S. & Wyllie, P. J. (1993) Experimental interactions of granitic and basaltic magmas and implications for mafic enclaves. *Journal of Petrology* **34**, 491–517.

Watson, E. B. (1982). Basalt contamination by continental crust: some experiments and models. *Contributions to Mineralogy and Petrology* **80**, 73–87.

Watson, E. B. (1994). Diffusion in volatile-bearing magmas. In: Carrol, M. R. & Holloway, J. R. (eds) *Volatiles in Magmas. Mineralogical Society of America, Reviews in Mineralogy* **30**, 371–411.

Watson, E. B. (1996). Dissolution, growth and survival of zircons during crustal fusion: kinetic principles, geological models and implications for isotopic inheritance. *Transactions of the Royal Society of Edinburgh: Earth Sciences* **87**, 43–56.

Wickham, S. M. (1987*a*). The segregation and emplacement of granitic magmas. *Journal of the Geological Society, London* **144**, 281–297.

Wickham, S. M. (1987*b*). Crustal anatexis and granite petrogenesis during low-pressure regional metamorphism: the Trois Seigneurs massif, Pyrenees, France. *Journal of Petrology* **28**, 127–169.

Wolf, M. B. & London, D. (1994). Apatite dissolution into peraluminous haplogranite melts: an experimental study of solubilities and mechanisms. *Geochimica et Cosmochimica Acta* **58**, 4127–4145.

Wolf, M. B., London, D. & Morgan, G. B., VI (1994). Effects of boron on the solubility of cassiterite and tantalite in granitic liquids. *Geological Society of America, Abstracts with Programs* **26**, pp. 450.

Zeng, Q., Nekvasil, H. & Grey, C. P. (2000). In support of a depolymerization model for water in sodium aluminosilicate glasses: information from NMR spectroscopy. *Geochimica et Cosmochimica Acta* **64**, 883–896.

Zhang, Y., Walker, D. & Lesher, C. E. (1989). Diffusive crystal dissolution. *Contributions to Mineralogy and Petrology* **102**, 492–513.